UNSTABLE WETTING FRONTS OF IMMISCIBLE FLUIDS DURING INFILTRATION IN POROUS MEDIA

Submitted as a partial fulfillment of Master degree

prepared by

Tsuhsin Lin

Hydrology Program
Department of Geoscience
New Mexico Institute of Mining and Technology

May, 1995

Table of Content

List of Figures

List of Tables

Abstract.

Three dimensional experiments of wetting front instability have been carried out in columns filled with perlite sands by applying diesel fuel at the column surface through an infiltration cylinder with a stainless steel plate of a uniform pore size attached at the bottom. The edge effect was avoided by restricting the infiltration area to be less than the cross-sectional area of the column. The infiltration was controlled at a rate less than the saturated hydraulic conductivity to trigger fingering. Observed finger widths increase as the sand becomes finer. The number of fingers observed in the coarse sand is higher than in the finer sand. The prediction for finger width based on linear stability theory are not applicable for our experimental results. It is difficult to derive a conclusive explanation from the observed wetting patterns between diesel and water experiments. The reason is essentially the inability to control many factors affecting experiments based on available facilities. The observed fingers may indicate that film flow plays a more important role in diesel experiments than in water experiments after halting the fluid supply, while the pore filling process is essentially stopped. Thus, there is less opportunity for instability to be observed in diesel experiments than in water experiments. The Miller scaling theory does not include the wettability effect which should be considered in comparison of wetting patterns for different liquids. The three-dimensional reconstructed images of fingers indicate that image analysis is a useful tool to study the observed phenomena compared with only a series of two-dimensional pictures. From image analysis, we can derive more useful information and more objective finger widths.

INTRODUCTION

The major cause for groundwater pollution is leaching of contaminants from the soil surface through the vadose zone into the groundwater. Recently, pollution by organic immiscible contaminants is receiving much interest. Unlike miscible solutes, it is still not well understood in which manner immiscible organic contaminants are transported through the soil (Mercer and Cohen, 1990). In a review and assessment of multiphase flow and transport models for organic chemicals, Abriola (1988) stated that 'this field is still in its infancy'. Even six years later, we still consider it in the same way.

One important question which must be answered for a good understanding of immiscible fluid infiltration into soil concerns the stability of the immiscible fluid wetting front in field soils. Kueper and Frind (1988) concluded in an overview of immiscible fingering in porous media that natural porous media contain heterogeneities at a fine enough scale such that no distinction need be made between stable and unstable displacements. This viewpoint appears to be generally accepted without substantiation through laboratory or field studies. Nevertheless, recent laboratory and field evidence (Glass et al. 1987, 1989a, 1989b, 1989c, 1990, and 1991; Hendrickx et al. 1991 and 1992) demonstrate that instability of immiscible fluid flow must be considered seriously. Lumping the effects of the naturally occurring heterogeneities of field soils with the effects of unstable wetting fronts will not lead to a proper understanding of the transport mechanism of immiscible fluids in the vadose zone. The work of Glass, Hendrickx, and other investigators (Baker and Hillel, 1990; Diment et al., 1985; Starr et al., 1978; Van Ommen et al., 1989; Van Dam, 1990) is beginning to convince most hydrologists and soil scientists that fingering in field soils is a process which must be taken into account.

The objective of our research is to conduct immiscible fluid infiltration experiments in sand columns and to study the effects of infiltration rate and grain size on stability of wetting front of a low volatile hydrocarbon liquid, such as diesel. In this paper we present experimental results of wetting front instability of immiscible fluids during the downward transport process and comment on the application of linear stability theory. Since Yao and Hendrickx (1993) have indicated that the linear stability theory did not provide a correct prediction of their experimental results at low flux rates, we concentrate the experiments at low flux rates. From the scaling point of view, we also compare our results with those observed during water experiments within the same porous media.

BACKGROUND OF THEORY

Saffman and Taylor (1958) identified three factors influential in determining the stability of a steady, constant velocity, one-dimensional downward displacement of one fluid by another in a homogeneous, isotropic porous medium. The three factors are the difference of fluid density (ρ), the difference of fluid viscosity (μ), and the interface velocity (U). Their result indicates that the displacement is unstable if the following inequality satisfied:

$$kg(\rho_1-\rho_2)-\theta U(\mu_1-\mu_2) > 0 \qquad (1)$$

where k is the permeability of the medium, θ is the effective porosity that is the pore volume available for fluid transport, g is the gravitational constant, and subscript 1 indicating displacing fluid and 2 displaced fluid. Several assumptions are made to derive this criterion: the fluids are incompressible, Darcy's law is valid, the mixing between two fluids at the interface is negligible, and θ is the same for each fluid. Consider the case that water (fluid 1) is displacing air (fluid 2), the velocity (U) of the interface is constant, and the air experienced little compression. Then, the density difference is destabilizing, and that of viscosity is stabilizing. In a two-phase flow system such as water and air, or oil and air, since the viscosity and density of both fluids are much higher than that of air, Eq(1) can be simplified as

$$K_S > \theta U \qquad (2)$$

where K_S is the saturated hydraulic conductivity of the medium and θU is simply the flux, q_S, through the system. Therefore, Eq(2) predicts that all infiltration flows in an air filled porous medium where liquid is supplied at a rate less than the saturated conductivity are unstable. Hill and Parlange (1972) first applied the inequality, Eq(2), and conducted a series of experiments to demonstrate the instability of the macroscopic water and air interface. They termed the instability, "wetting-front instability", and the phenomenon has been the subject of numerous research efforts.

Parlange and Hill (1976) derived an equation, Eq(3), to predict two-dimensional finger width by perturbing the front to find the relation between the fastest growing disturbance and the finger width based on the linear stability theory.

$$D = \frac{\pi S^2}{K_s(\theta_s - \theta_i)} \frac{1}{(1 - R_s)} \qquad (3)$$

where D is the finger diameter (cm), S is the sorptivity of media for water at water entry value ($cm/s^{0.5}$), K_S is the saturated hydraulic conductivity (cm/s), θ_S is the saturated water content (-), θ_i is the initial water content (-), and $R_S = q_S/K_S$ is the ratio of system flux to saturated conductivity. Glass et al. (1990) extended the study to three-dimensional fingers and derived the equation (4).

$$D = \frac{4.8 S^2}{K_s(\theta_s - \theta_i)} \frac{1}{(1 - R_s)} \qquad (4)$$

The difference between two equations is only the coefficient, i.e. the ratio of finger width seen in two-dimensional experiment and in three-dimensions is π/4.8.
Glass et al. (1989a) applied dimensional analysis and Miller scaling theory (Miller and Miller, 1956) and derived the finger width in term of system parameters, Eq(5).

$$D = \frac{\sigma}{\rho g m} \frac{S_*^2}{K_{s*}(\theta_s - \theta_i)} F(R_s) \qquad (5)$$

where $F(R_S)$ is a function to be determined by experiment. K_S* and S_* (both dimensionless) are found by

$$K_s = \frac{\rho g m^2}{\mu} K_{s*} \tag{6}$$

$$S^2 = \frac{\sigma m}{\mu} S_*^2 \tag{7}$$

where ρ is the fluid density (g/cm^3), σ is the fluid surface tension (g/cm^2), μ is the fluid dynamic viscosity (g/cm/s), g is the gravitational constant (cm/s^2), and m is a microscopic length scale of the porous medium (cm). This value is usually taken as the mean grain size. If we move all parameters on the right-hand side of Eq(5) except K_S*, S_*, and $F(R_S)$ to the left-hand side, a normalized finger width is derived as Eq(8). Note this value is scaled by the properties of the fluid and the medium.

$$D_* = D\frac{\rho g m(\theta_s - \theta_i)}{\sigma} = \frac{S_*^2}{K_{s*}} F(R_s) \tag{8}$$

The function $F(R_S)$ in Eq(5) and Eq(8) can be related to Eq(4) to give

$$F(R_s) = \frac{A}{(1-R_s)^B} \tag{9}$$

where A and B are constants to be determined by experiments. Glass et al. (1991) compared their experimental results and concluded that the value of A, 4.8, and B equal one gave a reasonable fit for three-dimensional finger widths. Since these values were derived from the linear stability analysis by imposing a perturbation at the front with a shape of the first kind of Bessel function, they might not be applicable to other experiments performed in a different system. Nevertheless, we will test if they can be applied to our experiments. If we move $F(R_S)$ to the left-hand side of Eq(8), then a material constant, S_*^2/K_S*, is derived. We will also test if our experimental results reveal this material constant.

The Miller scaling concept requires that K_S*, and S_* be identical functions between two similar porous media. Based on this assumption, we may apply Eq(6) and Eq(7) to derive the invariant K_S* and S_* from water experiments in one porous medium and then predict finger size for other fluids in a similar porous medium. If R_S for some fluid in two media is the same, then, finger diameter is expected to be inversely proportional to the microscopic length scale, m, from Eq(5). That is a bigger finger should appear in finer sands for the same R_S. Also, for the same R_S but two different fluids, finger size is proportional to the surface tension and inversely proportional to the product of the fluid density and the medium's microscopic length scale. For example, the finger width for infiltrating diesel fuel is related to that of infiltrating water by

$$\frac{D_{diesel}}{D_{H_2O}} = \frac{\sigma_{diesel}\rho_{H_2O} m_{H_2O}}{\sigma_{H_2O}\rho_{diesel} m_{diesel}} \frac{F(R_{s@diesel})}{F(R_{s@H_2O})} \tag{10}$$

Yao and Hendrickx (1995) have conducted a series of water experiments on perlite and quartz sand and observed different behavior from prediction based on the above theories, i.e. Eq(4). We

will use the same porous media but injecting diesel and test if Eq(4) is applicable. If the prediction for finger width of diesel is also not consistent with experiments, we then compare results of diesel and water for same flux ratio, R_S, to test Eq(10). If it is also not applicable, this may indicate that the assumption of the Miller scaling theory is not valid for the porous media used in our experiments.

MATERIALS AND METHODS

The infiltration mechanism of stability experiments have been carried out by Glass et al. (1989b, 1989c, 1990, 1991) by ponding on a restrictive layer to simulate a surface spill of contaminants. Yao and Hendrickx (1995) used a sprinkler system to mimic the natural rainfall. We used an infiltration cylinder with a porous plate attached at the bottom of the cylinder to simulate the leakage from underground storage tanks due to corrosive tank material. Since air dry sands were used for experiments, we had two immiscible fluids: test fluid and air.

Materials.

The experimental sand is crushed volcanic perlite which is mainly composed of silica (75% weight by chemical analysis). The crushed particles are separated by sieving into four categories: 14-20 (1.41-0.84 mm), 20-30 (0.84–0.59 mm), 30-40 (0.59-0.42 mm), and 40-60 (0.42-0.25 mm), based on U.S. sieve number. The specific density of the perlite is 2.2 g/cm^3 which is lower than the specific density of field soils (2.65 g/cm^3). The bulk density of the four sand fractions is 1.25±0.01 g/cm^3. We decided to use perlite because (1) it produces a porous medium similar to field sands and (2) it is provided to us by the Grefco Mine in Socorro, NM, without costs.

The experimental hydrocarbon is diesel (grade no. 2) from the gas station of the Physical Plant at the New Mexico Institute of Mining and Technology. The original source is the Navajo Refining Company in New Mexico. The viscosity of diesel was measured by using the Cannon-Fenske Routine viscometers. The procedures are described in ASTM under sections D445-88 and D446-89a. The formula used to derive the viscosity of regular petroleum product at a test temperature different from the calibration temperature is described in the ASTM under section D341-89. The relative kinematic viscosity of diesel is 4.6 at 22°C. Most of experiments were conducted outside under the shade of an open trailer. The temperature for each experiment was taken as ambient temperature in the trailer with the sidedoor opened. The viscosity dependency of diesel on temperature was measured and is shown in Fig. 1.

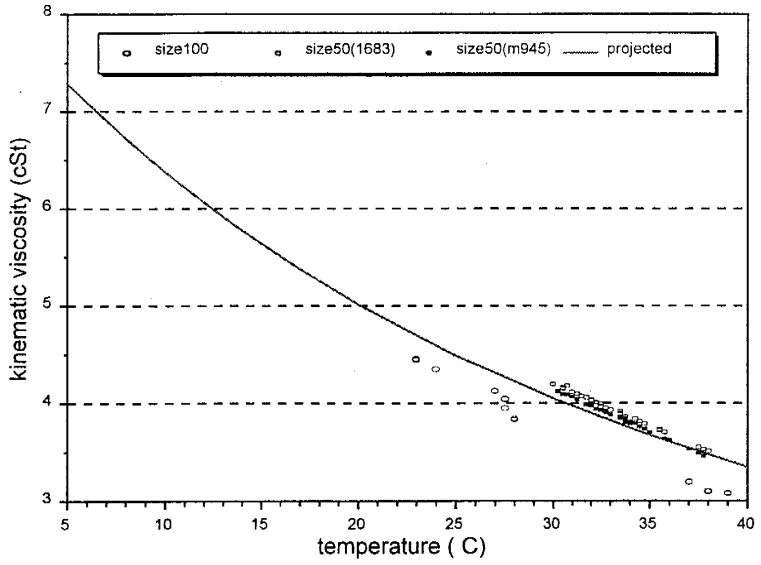

Fig. 1 Viscosity dependence of diesel on temperature by Cannon-Fenske viscometer, where the indicated size is for measuring different ranges of viscosity stated in ASTM

The surface tension of diesel was measured with the ring method on the FISHER Surface Tensiometer (ASTM D1590-60). The diesel-air interfacial tension is approximately 30 dyne/cm. The density of diesel is 0.85 g/cm^3. The density does not show a significant variation on temperature between 20 to 35°C. The surface tension decreases slightly with temperature (Fig. 2).

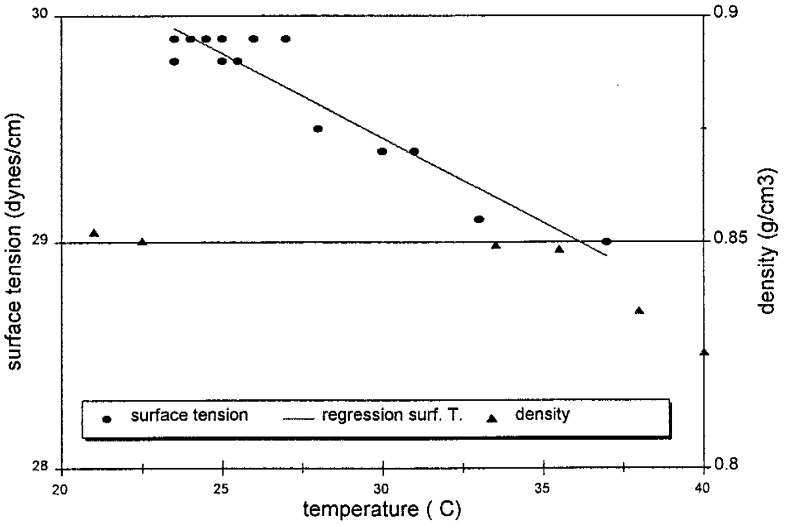

Fig. 2 Surface tension and density dependence of diesel on temperature with the linear regression for surface tension

We also measured the evaporation of diesel during a normal operation period of three hours, by monitoring the weight change of diesel in a beaker open to the atmosphere. The results confirmed that diesel is a low volatile organic liquid (Fig. 3).

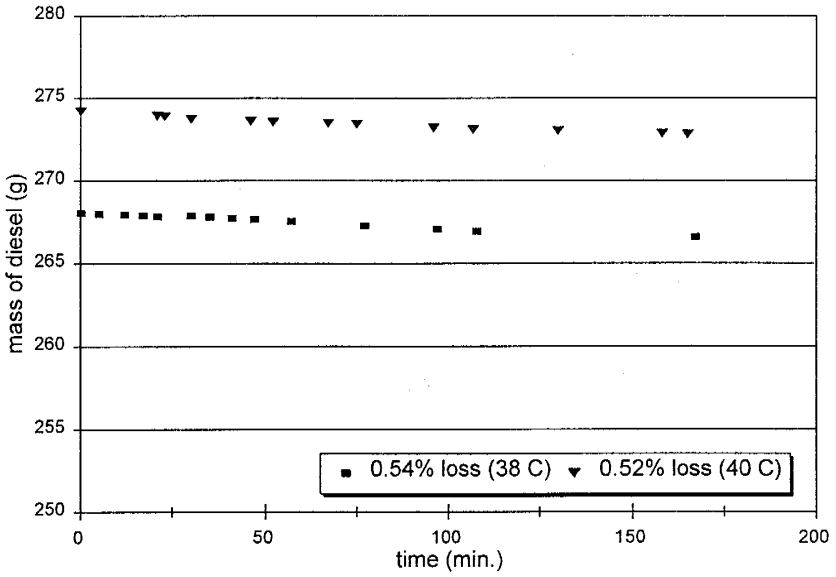

Fig. 3 Weight change of diesel in open beaker through evaporation during experiments

Assuming wettability of diesel and water in perlite are the same, then sorptivity can be scaled by the surface tension and viscosity of each fluid. Therefore, the sorptivity for diesel is interpreted from water experiments by using Miller and Miller scaling theory; i.e. find $S*$ from water experiments. The dimensionless $S*$ was then calculated as 0.0167 for the 30-40 mil perlite sand. Table 1 lists the fluid and transport properties for both diesel and water for comparison. Cost effectiveness forced us to use diesel instead of a purer laboratory oil. In addition, diesel is a common contaminant from surface spill or leakage from underground storage tanks (Ashley, et al. 1994; Lemonick, 1988).

Table 1 Fluid and transport properties

Fluid prop. at 21-22°C	Diesel			Water	
density (g/cm^3)	0.85			1.00	
dyn. viscosity (cP)	3.90			0.98	
kinematic visc. (cSt)	4.58			0.98	
surf. tension (dyne/cm)	30			72	
Perlite sand transport properties	Ks (diesel) (cm/s)	Ks*(water) (cm/s)	intrinsic perm. (cm^2)	sorptivity*(water) ($cm/s^{0.5}$)	mean grain size (mm)
14-20 mil	0.067	0.33	3.31E-06	0.22	0.840
20-30 mil	0.042	0.20	2.00E-06	0.28	0.584
30-40 mil	0.026	0.13	1.30E-06	0.29	0.408
40-60 mil	0.014	0.07	7.01E-07	0.25	0.279

* Water experiment data are derived from Yao (1993)

Sand Packing Procedure.

The experiments were conducted in PVC columns with a diameter of 30 cm. Each column consists of 45 to 50 one-cm high PVC rings that were stacked on a wood base. The column was filled using a 65-cm high PVC randomizer chamber with one porous plexiglas plate at 40 cm height, and two coarse wire mesh grates: one at the bottom and one at 10 cm above the bottom. To assure a uniform and compact sand packing, we overfilled the column to add additional weight. After completion of this process the top overfilled sand was removed. The filling procedure is after Glass et al. 1990.

Diesel Infiltration Method.

In order to study the relationship of finger size and flow rate, we built an infiltration cylinder to control the flow rate as steady as possible during infiltration. A 5-cm high plexiglas cylinder was sealed on the top with a plexiglas plate and a stainless steel porous plate, 18-cm in diameter, was attached at the bottom. The porous plate was cut from a 8.5*10 inch Mott 316L SS sheet with a thickness of 0.062 inch (1.57 mm). It serves the same function as a fine sand layer and we assume it would increase the uniformity of diesel injection. The cylinder was connected with a diesel tank by a 3/8 inch (O.D.) Tygon tubing, which was routed through a MasterFlex pump. We measured the flow rates both before and after the diesel was applied to the sand column. The total injected volume for each experiment ranged from 0.8 to 1.5 liter. Fig. 4 illustrates the experimental setup.

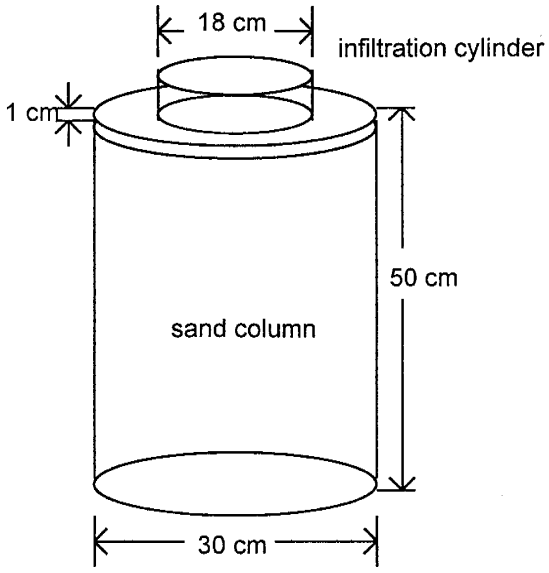

Fig. 4 Illustration of experiment setup

Measurement of Diesel Retention Curve.

Previous work by Glass has shown that the fluid retention characteristic is an important parameter affecting the stability of the flow in a porous medium. We obtained the relationship between diesel content and diesel pore pressure in a unsaturated sand column through a capillary rise experiment in 20 stacked 1-cm high PVC rings with 7.75 cm inner diameter. The bottom

ring was attached to a porous plexiglas plate by epoxy and a filter paper was fitted in this bottom ring before packing the sand. The sand column was placed in a pan with the diesel level higher than the bottom ring. After allowing the sand to absorb the diesel for three days, the wetted sand from each ring was weighed. The wet samples were dried in the oven for two days at 150°C, and weighed again. The difference between the two weighted measurements is used to calculate the diesel mass absorbed by the sand in each ring. The height of the ring above the diesel level in the pan was converted to the pore pressure by multiplication with the specific density of the diesel.

Measurement of Diesel's Saturated Conductivity.

The measurement was conducted in a glass column of 5 cm inner diameter and 5.5 cm in length. Sand was poured into the column through a small randomizer made of PVC pipe with the same inner diameter as the glass column. Carefully packing procedure was followed to ensure that sand was as compact as possible. Both ends of the sand column were supported by a two-layer metal mesh with cheese cloth sandwiched in between. In order to eliminate the boundary effect at the contact of tubing and the glass column, we maintained a free drainage chamber about one cm long on both ends of sand column. The column was vacuumed for half hour to prevent the air entrapment. The constant head method was applied to derive the saturated conductivity.

Image Analysis of Experiment's Pictures.

For each experiment, a series of pictures capturing the wetting pattern at different depths were scanned by a color scanner. The image file with a resolution of 300 pixels/inch for each picture, which corresponds to about 25 pixels for every centimeter in the physical system, was created by using a commercial software, Adobe Photoshop. The area outside of the sand column was cut from the scanned image, therefore, the draft image only showed the cross section of sand without the PVC ring. The wetted area was selected and seperated from the dry area based on the color similarities of adjacent pixels. Then, we changed the color in the selected area (wetted) into black and the color in the dry sand into yellow. The background color, i.e. the area outside of sand column, is in white. The new image file was saved to a lower resolution of 180*180 pixels for each slice, about 6 pixels per physical centimeter to reserve the hard disk space.

Average fluid saturation

A histogram representing the tonal distribution was created for the area of the sand column, in which the program counts the total pixels in black and yellow and the percentile for black pixels was derived. The percentile for black pixels indicates the wet fraction of the cross sectional area of the column. The wet fraction was plotted against the column depth, and a simple linear interpolation was used to derive the fraction at depths where no picture was taken. The total wet volume was calculated by summing up the wet fraction of 707 cm^3 (radius, 15 cm, and height, one cm) at each depth. This volume includes the volume occupied by the fluid, the sand, and also the air if the sand is not fully saturated (most of the cases in our experiments). Since we know the injection rate and time, the total injected volume is known. An average volumetric fluid content or saturation can be derived by dividing the injected volume by the pore volume in the wet region as shown in Eq(11).

$$DAS = \frac{V_{fluid}}{V_{wetpore}} = \frac{q_s A_{cylinder} t_{inj}}{\phi \sum_{1}^{n} f_{wet} A_{sand}} \quad . \qquad (11)$$

where DAS is the depth-average saturation, V_{fluid} is total volume of injected fluid (cm^3), $V_{wet\ pore}$ is total pore volume in the wet region (cm^3), q_s is the system flux rate (cm/s), $A_{cylinder}$ is the cross-sectional area of the infiltration cylinder (cm^2), t_{inj} is the injection time (s), ϕ is the porosity of the porous medium (-), f_{wet} is the wet fraction at each depth, and A_{sand} is the cross-sectional area of the sand column (cm^2). This method is applicable only for experiments in which the fluid does not reach the bottom of the column, and gives only a depth-average saturation.

Three dimensional finger rendering

After generating a series of two dimensional image files, we reconstructed the three dimensional finger by using another commercial software, Spygalss Dicer. Since Dicer creates one volumetric pixel per data element by default, the size in the vertical dimension will be equal to the total number of slices, generally 15~24 slices for each experiment. However, in the horizontal dimension, the size in each direction is 180 (180 pixels), we need to enlarge the vertical display size by a factor between 4 and 6 and reduce the horizontal display size by a factor of 1/2 to make the resulting 3D image approximate the real dimension of the column. Spyglass Dicer then interpolates the actual data between slices by using a linear method. After rendering the 3D volume image, we can use the slice tool to view the finger pattern in the slice at any angle. We are especially interested in the vertical slice, because we can derive information which is difficult to gain if only 2D pictures are available, such as how long fingers persist, how they connect with each other, and whether or not converging and diverging fingers exist.

RESULTS AND DISCUSSION

Retention Curve Experiments.

The wetting curves of diesel capillary rise experiments in four sand sizes were analyzed by using RETC (RETention Curve) program and the best fitted parameters are listed in Table 2. The fine sand has a higher retention than the coarse sand as indicated by the air-entry suction value. The α values for diesel is almost twice as for water, therefore, it shows the air-entry value for diesel is near half of that for water, since the air-entry value is taken as $1/\alpha$.

Table 2 Physical parameters of the perlite sand from fitting retention curves

Perlite sand size	α (cm^{-1}) (diesel)	α* (cm^{-1}) (water)	n (diesel)	n* (water)	ψ_e(cm) (diesel)	ψ_{e*}(cm) (water)	ratio of ψ_e
14-20 mil	0.372	0.188	3.74	3.48	2.02	3.55	1.76
20-30 mil	0.241	0.131	4.53	4.50	3.21	5.10	1.59
30-40 mil	0.185	0.092	4.75	5.07	4.18	7.30	1.75
40-60 mil	0.148	0.062	4.94	5.19	5.10	11.4	2.24

α and n are empirical parameters by fitting van Genuchten equation;

ψ_e (air-entry suction value) is derived from Brooks and Corey equation;

* values for water derived from Yao (1993)

Conductivity Experiments.

The saturated conductivity for each sand is listed in Table 1. We kept the head difference in the range between 3 and 10 cm for a 4 cm long sand column. Since there were free drainage chambers on both ends of the sand column, the entrapped air finally accumulated in the buffer rather than in the porous media, so as to mitigate the effect of entrapped air bubbles in the media. The difference of the intrinsic permeability for each size of sand derived from diesel and water's saturated conductivity is less than 7% (see Table 3), which is reasonably consistent.

Table 3 Comparison of transport properties between diesel and water at 22°C

Perlite sand transport properties	Ks (diesel) (cm/s)	Ks (water) (cm/s)	intrinsic perm. from diesel (cm^2)	intrinsic perm. from water (cm^2)	difference %
14-20 mil	0.067	0.33	3.134E-06	3.305E-06	5.18
20-30 mil	0.042	0.20	1.965E-06	2.003E-06	1.93
30-40 mil	0.026	0.13	1.216E-06	1.302E-06	6.60
40-60 mil	0.014	0.07	6.549E-07	7.011E-07	6.60

The intrinsic permeability derived from the saturated conductivity of diesel was less than that derived from water. This may be due to the different setup for measuring the conductivity of each fluid even though we used the same constant head method. The consistency indicates that the conductivity for different fluids can be scaled by the fluid's properties, i.e. density and viscosity, to derive the intrinsic permeability which is only a variable dependent on the porous medium. In convention, we assume the porous media contain uniform grains, and further derive the relation between permeability and the grain size of the media to be $k = k_* m^2$, where k is permeability, k_* is a constant or shape factor, and m is the mean grain size. This relation is also used in Eq(6). However, we found that the permeability for perlite sand is best fitted by a power of 1.4 to the mean grain size instead of 2 and the resulting constant, k_*, equals $1.1*10^{-4}$. The decline in the exponent is consistent with the observation by Shepherd (1989). He used 18 published studies to relate conductivity and mean grain size and found that both the shape factor and the exponent declined for sediments that were less texturally mature and were least for consolidated sediments. Particle shape of perlite sand used for our experiments is different from natural sediments in various aspects. Angularity of perlite sand may affect compactness and rearrangement during infiltration, and affects effective porosity. The structure may trap air more easily and thus reduce K_S compared to a natural sand with a comparable grain size.

Continuous Source Infiltration Experiments.

A total of 48 diesel experiments were conducted including 17 trials for 14-20 sand, 15 trials for 20-30 sand, 9 trials for 30-40 sand, and 7 trials for 40-60 sand. A total of seven control experiments by injecting water were also carried out for similarity purpose. Appendix 1 lists detailed information for diesel experiments and the predicted finger diameter based on the linear stability theory. Appendix 2 lists detailed information for water control experiments. Typical diesel experimental results for 14-20, 20-30, and 30-40 sand are included in Appendix 3, 4, and 5, respectively. Appendix 6 shows a typical result for the water control experiment. The complete experimental pictures were held by Dr. Hendrickx. Instability did not appear in all experiments with a supply flux less than the saturated conductivity as expected from the linear stability theory. Fingers often occurred in coarse sands, but never in the finest sand (40-60 mil)

tested in our experiments. This might be limited by the size of 30-cm diameter column and the injection area restricted by the infiltration cylinder with a radius of 9 cm. Finger size was determined by visual examination of the plot of the finger diameter versus depth and taken as the depth average reading (Fig. 5).

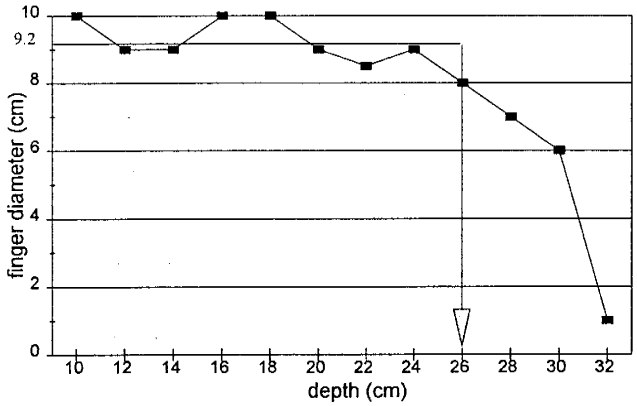

Fig. 5 Distribution of finger width versus depth with an average width of 9.2 cm between the depth of 10 and 26 cm

If there were more than one distinctive isolated finger dominating the flow region, then we averaged the size of the similar fingers (ratio of each finger size compared to the average one falling between 0.8-1.3) which lasted for a substantially long distance (say six to ten cm) as representation for the corresponding flow rate. This range is subjective for which we simply imply the substantially bigger finger (ratio of finger size higher than the prescribed range) was the merging result of several fingers, or the substantially smaller finger was at the tip of the front, thus disregarded in the derivation of representative finger size. If no distinctive finger formed, like in the 30-40 mil sand fingers were found usually overlapped with each other, then we tried to trace the curvature of the wetting pattern in order to determine the finger size as shown in Fig. 6.

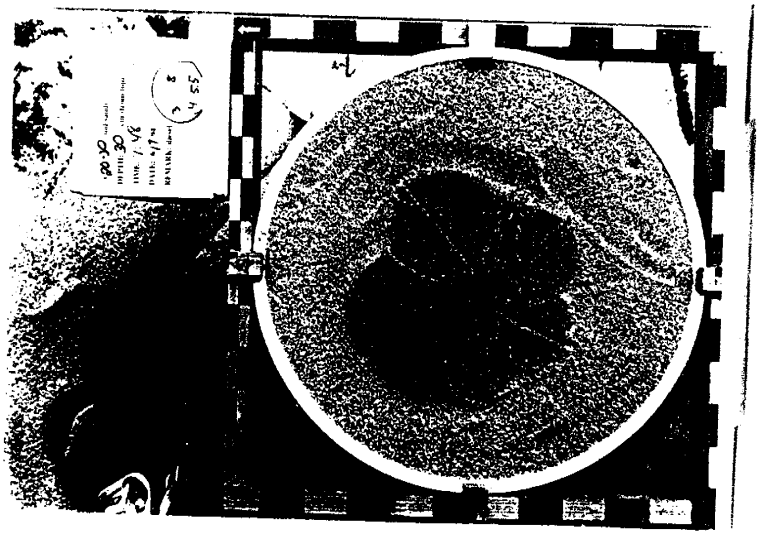

Fig. 6 Delineation of finger curvature

Fig. 7 is the plot of finger diameter versus flux ratio. The plot shows the size of observed fingers decreased with increasing the size of sand, which is consistent with present theories, as depicted in Eq(5). The number of fingers observed increased with the size of sand as indicated from Appendix 1. This is also consistent with observations from previous works of Glass et al. (1989b, 1989c, 1991) and Yao and Hendrickx (1993).

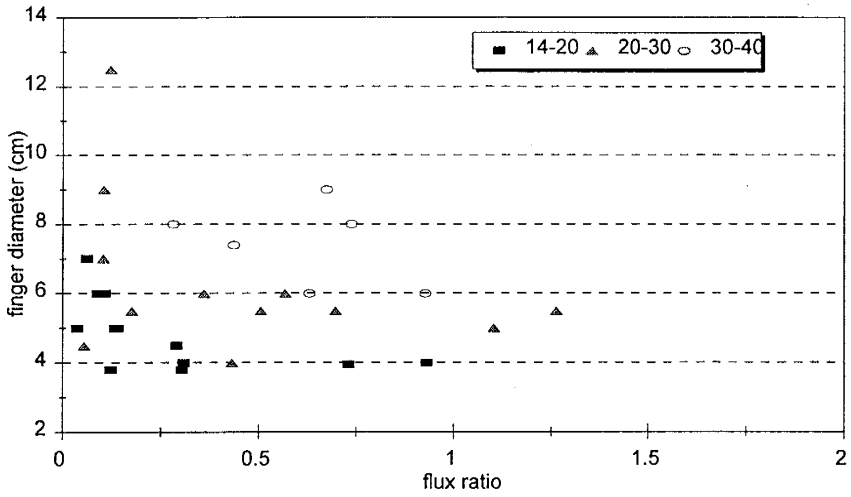

Fig. 7 Finger size versus flux rate for diesel experiments

However, we have observed an increasing size with decreasing infiltration rate. This phenomenon was not reported in previous experimental work by Glass et al. (1989b, 1989c, 1991) until Yao and Hendrickx (1995) indicated the trend in their water experiments.

Observed Finger Size and Prediction

Fig. 8 plots the normalized observed (data point) and predicted fingers (solid curve) versus flux ratio, and the value can be found in Appendix 1 for each experiment. The normalized finger size was calculated by Eq(8) for both diesel and water, and the predicted finger diameter was derived by taking $S_* = 0.01675$ and $K_{S*} = 7.8*10^{-4}$, from 30-40 mil sand experiments. Data of water experiments were derived from Yao (1993) except the control experiments. Most of observed finger sizes were larger than those predicted at the low flux region and smaller at the high flux region. This inconsistency for diesel and water (Yao and Hendrickx, 1993) from prediction shows that the present theories based on the perturbation of a Bessel function is not applicable for our experiments. The smaller fingers observed at high flux ratio can be attributed to our experimental setup. Since the infiltration area is smaller than the total cross-sectional area of the column, diesel can infiltrate horizontally so that the wet area is expanded, thus the actual infiltration rate is lower than the system flux rate. We did not have any in-situ monitor device to record the speed of the advancing front, so the initial system flux instead of the finger velocity was used in our analysis.

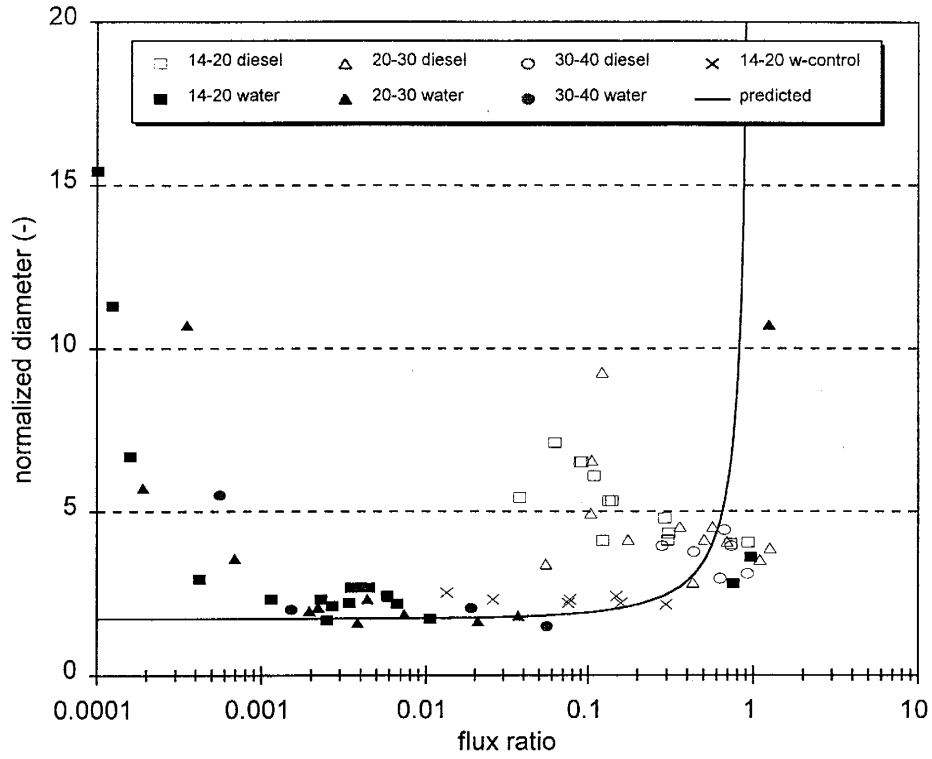

Fig. 8 Normalized observed and predicted finger size for both diesel and water experiments (water experiment data derived from Yao, 1993)

Comparison of Finger Size Between Diesel and Water Experiments.

The control experiments (data with the cross mark in Fig. 8) by using the infiltration cylinder show a consistent pattern as those from Yao (1993) by using a sprinkler system. If comparing both diesel and water experiments with a similar flux ratio, Rs, it reveals that the finger diameter is higher for diesel than water, which is contradicted by Eq(10). Since Eq(10) includes the scaling by fluid density, surface tension, microscopic length of the medium, and flux function, assuming the flux function is same for both liquids, even though we did not specifically derive the function, we expect the size from water experiments would be almost twice of that for diesel in the same porous medium. But the experiments show that diesel had larger fingers than water's at the similar flux ratio, around 0.7 to 0.9, as indicated by 14-20 sand, this finding leads us to believe there is other mechanism which we did not consider before. We suspect the bigger fingers at the low flux ratio were formed due to converging of several smaller fingers. However, the magnitude of the ratio at which fingers converge for diesel and water is different, almost three orders of magnitude smaller for water to show the increasing trend in finger size than diesel's. This phenomenon may be explained by the different extend of induced film flow on redistribution of fluid. Since the transport of diesel is slower than water, the time scale for film flow to take place is longer for diesel than for water. Therefore, the convergence of fingers is likely to occur in diesel experiments than water's. More detailed discussion is in the section of the transport processes following the section of the image analysis.

Image Analysis

By image analysis and mass balance calculation, we found that the diesel content in the wetted region was far less than saturation. In the 14-20 mil sand, one typical experiment had 26% of void volume occupied by diesel, i.e. saturation is 0.26. In another 20-30 mil sand column, diesel occupied only 35%. Fig. 9 shows the fraction of diesel-wet area along the column depth. Since the finger would continue to move while slicing the column, we did not take any small sample for measuring the diesel content at each depth in order to complete the slicing as soon as possible to prevent the further movement of fingers.

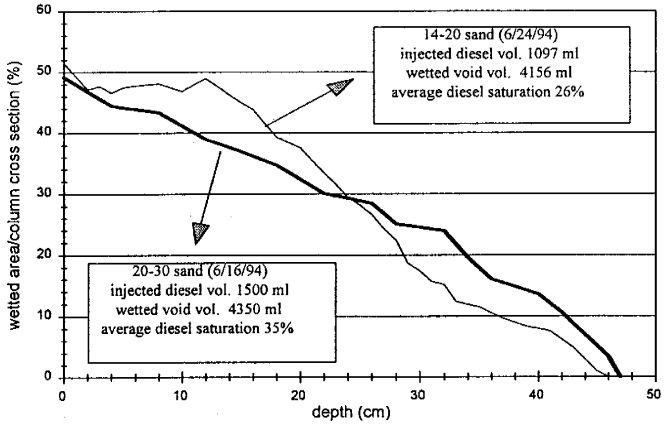

Fig. 9 Distribution of diesel-wet fraction versus column depth

Fig. 10 shows a three-dimensional rendering finger from a series of two-dimensional images scanned from experiment pictures. One can see the dry area disappears near the surface after the depth around two centimeters and finger splitting around the third horizontal slicing. The image analysis can help us to derive more useful information in term of finger structure and their interaction.

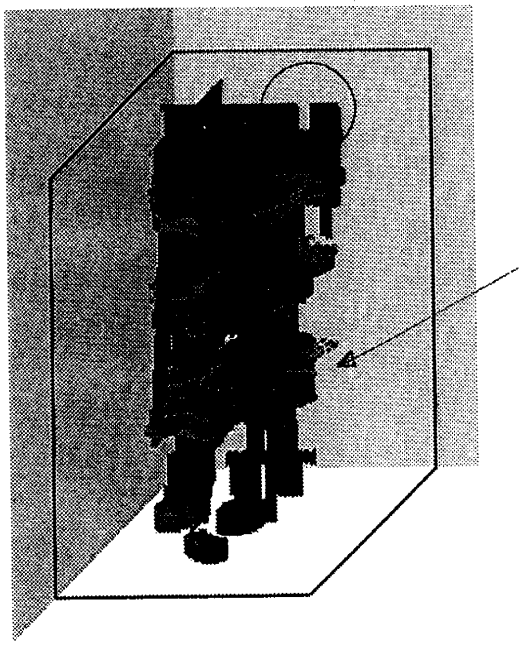

Fig. 10 Three-dimensional finger reconstructed from a series of two-dimensional images

Transport Processes

From observations of the wetting pattern, we may divide the flow process into two stages. These include (1) infiltration through the porous plate and (2) infiltration in the sand column.

(1) infiltration through the porous plate

Originally we assumed the injection of fluid through the plate could be more uniformly distributed than using a finer sand. Nevertheless, the plate is still a porous medium and retains the nature of heterogeneity in pore structure. This character accompanies with the air entrapped in the plate at the beginning of infiltration preselected the paths through which diesel first contacted the sand. The uniformity of injection may be affected by wetting history and residual oil in the plate as well as flux rate controlled by the pump. It was observed that if the flux was high enough, the flow became jet-like from numerous locations out of the bottom of the plate just like flow through a steady sprinkle system with small spaced syringes. This feature was well captured in the wetted pattern at the surface of sand column. Fig. 11(a) shows small bulges of sand (the mount shape was due to capillary) have formed with a distance about 1 cm from each other at the contact surface of the plate and sand after infiltration. This indicates the possible preferential paths of infiltration for diesel and reflects the initial perturbation imposed by the pore structure of the plate is finite. Nicholl et al. (1994) indicated their fluid application process initially introduces a characteristic perturbation wavelength of approximately 1.6 cm due to the syringe spacing. They concluded predictive models for finger width assuming growth from infinitesimal perturbations (linear stability theory) are not expected to be appropriate for fingers initiated from finite amplitude perturbations. This interpretation may explain why finger widths observed in the experiments cannot be predicted using the linear stability theory. Fig. 11 also reveals the variation of the wetted pattern at the surface of sand columns, which indicates various boundary conditions at infiltration. The dry area within the infiltration region near the top of columns indicates the air might be entrapped in the plate or could not escape after diesel front surrounding the area formed a continuos moving body at a depth around a couple of centimeters.

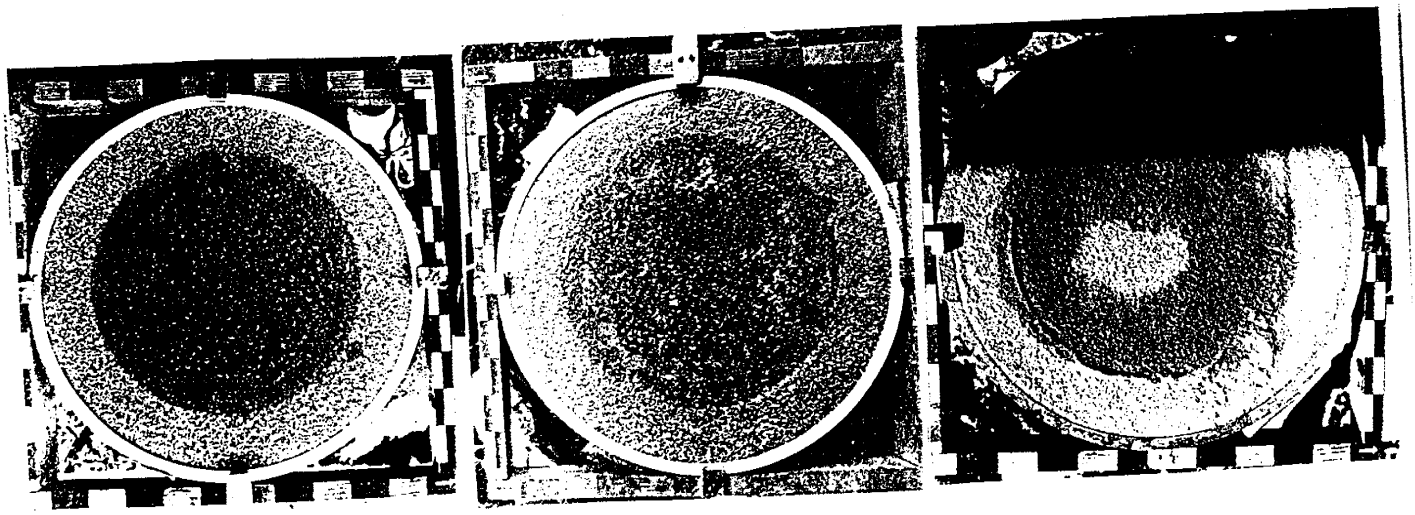

Fig. 11 (a) Small bulges on the surface of sand columns, (b) spotty dry surface, and (c) partially wet surface

(2) infiltration in the sand column

In this stage, there are two phases we need to consider where instability may be formed, the first phase is the period that diesel was continuously supplied, and the second phase is after diesel source was removed. During the diesel-injection period, the front was assumed to travel at a rate as the measured system flux rate, not saturated conductivity, because the diesel supply is controlled by a pump, not a ponding source. In this stage, viscous force and gravity force were the two dominant forces which determine instability. Since diesel was continuously supplied, the diesel content in the tail might not be too different from the tip. Diesel flow into the system before halting probably filled up a region at the top under the porous plate near a volume equal the flow volume divided by porosity. The volume of porous media wetted initially will be a function of the diesel supply flow rate, the higher the flow rate the smaller the volume of porous media wetted. The average saturation in the initially wetted region will be higher for higher flow rates. Topology of the wetting front at the end of diesel supply will be a function of supply rate, the higher the flow rate the flatter the front and the smaller the perturbations. For very low supply rates, one expects a single bulb with one major tip and this tip is lower than the front position of the high flow. What all this means is that supply flux systematically changed the frontal shape at the onset of redistribution. Since diesel wet area was expanded after infiltration, therefore, the real flow rate in the column was expected to be less than the measured initial flux rate. The is why even the initial flux ratio was higher than one, there was still instability shown in several cases. The moving front might be stable as seen in the two-dimensional experiments of Nicholl et al. (1994) because of damping of initial perturbations by capillary. After cessation of diesel supply, during the period of waiting and slicing the column, diesel in the sand column began redistribution as well as continuing downward movement. In this stage, film flow might be dominant, i.e. transport process around grains at grain contacts. This process is usually very slow and time scale required is longer than that for pore filling process during infiltration period. Since the conductivity of diesel is lower than water's and diesel is more viscous than water, we suspect the film flow process will be more important for diesel than for water. Therefore, smaller fingers converged into a bigger finger is more likely to occur in diesel experiments. On the other hand, the diesel content behind the tip of finger underwent a drying process while hysterisis started to play a significant role. During redistribution, the velocity of finger propagation was reduced and the finger width increased by lateral movements and/or film flow. This process in the three-dimensional system was hard to be quantified by analyzing the resulting two-dimensional pictures taken after the experiment. However, it was well observed by visual inspection in two-dimensional experiments by previous work of Glass et al. (1989b, 1989c), Selker et al. (1992a, 1992b), and Nicholl et al. (1994). The capillary force for diesel may overwhelm the gravity force to create more stable flow field than water, thus converging fingers due to capillary appeal at a higher flux ratio for diesel than water. Therefore, the unstable range in term of flux ratio for diesel is narrower than for water.

Sorptivity and Wettability

The sorptivity for diesel was interpreted from water experiments by using Miller and Miller scaling theory. From our experimental observations, we suspect the sorptivity of diesel cannot be interpolated from water's sorptivity. Since the wetting during diesel infiltration and the drying during redistribution, the process is dynamic and hysterisis is in effect. The sorptivity relationship between two fluids should also be a dynamic function. This function is hard to

defined and quantified with available instruments. Moreover, wettability factor is not included in the Miller and Miller scaling theory, whose validity is subject to futher investigation. The effect of wettability is further investigated by the capillary rise experiments and Young-Laplace equation. In Table 2, the α values for diesel is almost twice as for water, therefore, it shows the water-entry value for diesel is near half of that for water, since the water-entry value is taken as $1/\alpha$. This can be understood by considering the analogous relation of Young-Laplace equation describing the capillary rise with the surface tension and the density of fluid in Eq(12).

$$h = \frac{\sigma}{\rho g}\frac{2cos\theta}{r_m} \qquad (12)$$

where h is the capillary rise, σ is the surface tension, ρ is the density of fluid, g is the gravitational constant, θ is the contact angle, and r_m is the mean radius of the interface curvature. Take the surface tension of diesel as 30 dyne/cm and water, 72 dyne/cm, and the density of diesel, 0.85 g/cm^3, and water, 1 g/cm^3, we can derive the ratio of the capillary rise as Eq(13).

$$\frac{h_{water}}{h_{diesel}} = \frac{\sigma_{water}\rho_{diesel}}{\sigma_{diesel}\rho_{water}}\frac{\cos\theta_{water}}{\cos\theta_{diesel}} \qquad (13)$$

which is equal to 2.04*cosθ(water)/cosθ(diesel). If assuming the simple Young-Laplace relation for capillary tube is applicable to porous media and r_m is the same for both fluids, and take the ratio of the air-entry value after scaled by the density of each fluid as the ratio of the capillary rise, we may derive the contact angle for water is bigger than that for diesel since cosθ(water)/cosθ(diesel) is less than one, ranging from 0.66 (for 20-30 sand), 0.73 (for 14-20, 30-40 sand) to 0.93 (40-60 sand). This means diesel is more wettable than water for perlite sand. If we take this ratio into account and modify the non-dimensional equation of Eq(8), i.e. inserting cosθ in the denominator. The resulting normalized fingers for diesel and water become closer, however, they are still not collapsed together. Based on this finding, we have done contact angle measurements for both diesel and water on glass slides (Corning Micro Slide no. 2947). Since perlite sand consists of 75% of silica, we expect the contact angle measured on the glass slide which essentially composites silica can give us a qualitative indication of which liquid is more wettable on perlite's surface. We followed the procedure in Wei (1991) by using a Gelmont 2mL microburet and recorded the advancing and receding contact angles from a dynamic sessile drop. However, both advancing and receding angles for diesel and water did not show a significant variation on the glass slide (Table 4).

Table 4 Measurements of contact angle for diesel-air and water-air on glass slides

Contact angle	advancing (degree)	receding (degree)	after snap-off* (degree)	total sample number
diesel-air	12.2 ± 1.7	7.5 ± 0.6	2.2 ± 0.6	14
water-air	11.9 ± 2.3	8.3 ± 1.5	9.0 ± 1.4	18

* The angle was measured on the drop remaining on the glass slide after snap-off.

The small contact angles indicates that the glass slide is wettable for both diesel and water. Since the surface tension of diesel is less than water, the contact angle of diesel after snap-off is expected to be less than that for water which is consistent with observation. From the results of contact angle measurements, we cannot conclude that the glass slide is more wettable to diesel than water. In other words, we cannot imply that perlite is more wettable to diesel. Note that the Young-Laplace equation, Eq(12), governs the interrelationship between fluid interface curvatures, $2\cos\theta/r_m$, and the corresponding capillary pressures, $P_c=\rho gh$. It is difficult to differentiate the effect on the curvature from r_m and contact angle but their integrated result. Even though changes in curvature caused by difference in fluid densities are generally negligible at the microscopic (pore scale) level (Morrow and Melrose,1990), the boundary conditions of the interface need to be taken into account. Surface roughness, edge effects, and heterogeneity in surface wetting properties of porous media can all contribute boundary conditions that cannot be described by a unique contact angle (Morrow, 1990; Morrow and Melrose, 1990).

CONCLUSIONS

This project has initiated several experiment techniques to study flow of hydrocarbon liquid in sandy soils. We prevent the edge effect by restricting the infiltration area to be less than the cross-sectional area of the column and used a stainless steel plate instead of a real fine sand layer to have a better control on the infiltration rate. The sand column is packed in a stack of one centimeter height PVC rings, which can facilitate the slicing more easier and more uniform. We observed that finger widths increase as the sand became finer. The observed widths at low fluxes are usually larger than those predicted by using the equation derived from Glass for three-dimensional finger by using a linear stability analysis. This phenomenon may be due to convergence of several smaller fingers and caused by film flow and/or capillary force. In general, the number of fingers observed in the coarse sand is higher than in the finer sand. The observed finger widths indicate that the capillary force will dominate the gravity force sooner for diesel than for water, thus the size of diesel fingers was always larger than water's. The Miller scaling theory does not include the wettability effect which should also be a concern in comparison of wetting pattern for different liquids. The three-dimensional reconstructed images of fingers indicate that image analysis is a very useful tool to study the observed phenomena compared with only a series of two-dimensional pictures. From image analysis, we can calculate an average saturation and derive a more objective finger width.

Future Research

Fingers (unstable wetting) appear at a more restricted range of flux ratio for fine sand than for coarse sand. Therefore, the selection of infiltration rate should be more stringent for fine sand in order to study the instability phenomenon. Also, the size of the experimental column will determine the observable finger size. If we need to study the instability phenomenon in a fine sand, the column should be big enough to accommodate the finger. Since the lack of laboratory control and experimental facilities, we cannot control the fluctuation of temperature during experiments, this can be improved by running the experiment inside a building with good air circulation and proper temperature control device. The initial and boundary conditions

definitely influence the development of observed fingers, we should control all the factors to be as precise and consistent as possible. Note that diesel is still in the process of transportation during the slicing of the column, so if there is an instrument which can monitor the finger development in-situ and record it in a digital form, that will extremely assist our understanding of the phenomenon.

REFERENCES

Abriola, L.M. 1988. Multiphase flow and transport models for organic chemicals: a review and assessment. EPRI, Final Report, EA-5976, Research Project 2377-5. pp. 93.

Ashley, R.P., D.N. Lerner, and J.W. Lloyd. 1994. Distribution and degradation of diesel oil in the unsaturated zone following an oil spill on a chalk aquifer. J. of Hydrology, 159:43-59.

ASTM D445-88, Standard Test Method for Kinematic Viscosity of Transparent and Opaque Liquids, 1990 Annual Book of ASTM Standards, Volumes 05.01, 170-175.

ASTM D341-89, Standard Viscosity-Temperature Charts for Liquid Petroleum Products, 1990 Annual Book of ASTM Standards, Volumes 05.01, 140-144.

ASTM D446-89a, Standard Specifications and Operating Instructions for Glass Capillary Kinematic Viscometers, 1990 Annual Book of ASTM Standards, Volumes 05.01, 176-182.

ASTM D1590-60, Standard Test Method for Surface Tension of Water, 1990 Annual Book of ASTM Standards, Volumes 11.01, 230-232.

Baker, R.S., and D. Hillel. 1990. Laboratory tests of a theory of fingering during infiltration into layered soils. Soil Sci. Soc. Am. J. 54:20-30.

Chouke, R.L., P. van Meurs, and C. van der Poel. 1959. The instability of slow, immiscible, viscous liquid-liquid displacement in permeable media. Trans. Am. Inst. Min. Metall. Pet. Eng. 216:188-194.

Diment, G.A., and K.K. Watson. 1985. Stability analysis of water movement in unsaturated porous materials. 3. Experimental studies. Water Resour. Res. 21:979-984.

Diment, G.A., K.K. Watson, and P.J. Blennerhassett. 1982. Stability analysis of water movement in unsaturated porous materials. 1. Theoretical considerations. Water Resour. Res. 18:1248-1254.

Glass, R.J., J.-Y. Parlange, and T.S. Steenhuis. 1987. Water infiltration into layered soils where a fine textured layer overlays a coarse sand. Proc. Int. Conf. on Infilt. Devel. and Application, Yu-Si Fok, Editor. Water Resources Research Center, University of Hawaii, p. 61-81.

Glass, R.J., J.-Y. Parlange, and T.S. Steenhuis. 1991. Immiscible displacement in porous media: stability analysis of three-dimensional, axisymmetric disturbances with application to gravity-driven wetting front instability. Water Resour. Res. 27:1947-1956.

Glass, R.J., J. King, S. Cann, T.S. Steenhuis, and J.-Y. Parlange. 1990. Wetting front instability in unsaturated porous media: A three-dimensional study in initially dry sand, Transp. Porous Media, 5, 247-268.

Glass, R.J., T.S. Steenhuis, and J.-Y. Parlange. 1988. Wetting front instability as a rapid and far-reaching hydrologic process in the vadose zone. Journal of Contaminant Hydrology 3:207-226.

Glass, R.J., T.S. Steenhuis, and J.-Y. Parlange. 1989a. Wetting front instability: 1. Theoretical discussion and dimensional analysis. Water Resour. Res. 25:1187-1194.

Glass, R.J., T.S. Steenhuis, and J.-Y. Parlange. 1989b. Wetting front instability: 2. Experimental determination of relationships between system parameters and two-dimensional unstable flow field behavior in initially dry porous media. Water Resour. Res. 25:1195-1207.

Glass, R.J., T.S. Steenhuis, and J.-Y. Parlange. 1989c. Mechanism for finger persistence in homogeneous, unsaturated, porous media: theory and verification. Soil Sci. 148:60-70.

Hendrickx, J.M.H., and L.W. Dekker. 1991. Experimental evidence of unstable wetting fronts in homogeneous non-layered soils, in Preferential Flow: Proceedings of the National Symposium, edited by T.J. Gish and A. Shirmohammadi, p.22-31, American Society of Agricultural Engineers, St. Joseph, Mich., 1991.

Hendrickx, J.M.H., L.W. Dekker, and O.H. Boersma. 1992. Unstable wetting fronts in water repellent field soils. J. of Environmental Quality.

Kueper, B.H., and E.O. Frind. 1988. An overview of immiscible fingering in porous media. Journal of Contaminant Hydrology 2:95-110.

Lemonick, M.D. 1988. Nightmare on the Monongahela; a winter oil spill creates havoc from Pittsburgh to Wheeling. (Ashland Oil storage tank spills diesel fuel) Time v131, n3, Jan 18, 50-51.

Liu, Y., T.S. Steenhuis, and J.-Y. Parlange. 1994. Closed-form solution for finger width in sandy soils at different water contents. Water Resour. Res. 30:949-952.

Mercer, J.W. and R.M. Cohen. 1990. A review of immiscible fluids in the subsurface: properties, models, characterization and remediation. Journal of Contaminant Hydrology 6:107-163.

Miller, E.E. and R.D. Miller. 1956. Physical theory for capillary flow phenomena. Journal of Applied Physics 27:324-332.

Morrow, N.R. 1990. Wettability and its Effect on Oil Recovery, Journal of Petroleum Technology Dec. 1476-1484.

Morrow, N.R. and J.C. Melrose. 1990. "Applications of Capillary Pressure Data to the Determination of Connate Water Saturation," *Interfacial Phenomena in Oil Recovery*, N.R. Morrow (ed.), Marcell Dekker, New York City, 257-287.

Nicholl, M.J., R.J. Glass, and S.W. Wheatcraft. 1994. Gravity-driven infiltration instability in initially dry nonhorizontal fractures. Water Resour. Res. 30:2533-2546.

Philip, J.R 1969. Theory of Infiltration. Advanced Hydro-science 5:215-305.

Saffman, P.G. and G.I. Taylor. 1958. The penetration of a fluid into a porous medium or Hele-Shaw cell containing a more viscous liquid. Proc. R. Soc. London. A245:312-331.

Selker, J., P. Leclerq, J.-Y. Parlange, and T. Steenhuis. 1992a. Fingered Flow in Two Dimensions: 1. Measurement of Matric Potential. Water Resour. Res. 28:2513-2521.

Selker, J., J.-Y. Parlange, and T. Steenhuis. 1992b. Fingered Flow in Two Dimensions: 2. Predicting Finger Moisture Profile. Water Resour. Res. 28:2523-2528.

Shepherd, R.G. 1989. Correlations of permeability and grain size. Ground Water 27, 5:633-638.

Starr, J.L., H.C. DeRoo, C.R. Frink, and J.-Y. Parlange. 1978. Leaching characteristics of a layered field soil. Soil Sci. Soc. Am. J. 42:386-391.

Van Ommen, H.C., R. Dijksma, J.M.H. Hendrickx, L.W. Dekker, J. Hulshof, and M. van den Heuvel. 1989. Experimental assessment of preferential flow paths in a field soil. J. of Hydrology 105:253-262.

Van Dam, J.C., J.M.H., Hendrickx, H.C. van Ommen, M.H. Bannink, M.Th. van Genuchten, and L.W. Dekker. 1990. Simulation of water and solute transport through a water repellent sand soil. J. of Hydrology 120:139-159.

Wei, M. 1991. Wetting and non-aqueous phase liquid saturations in homogeneous porous media. Master Thesis. New Mexico Institute of Mining and Technology, Socorro, NM.

Weitz, D.A., J.P. Stokes, R.C. Ball, and A.P. Kushnick. 1987. Dynamic capillary pressure in porous media: origin of the viscous-fingering length scale. Physical Review Letters 59:26:2967-2970.

Yao, T., and J.M.H. Hendrickx. 1995. Wetting front stability in uniform soils under low infiltration rates. submitted to Soil Sci. Soc. Am. J. (in press).

Yao, T. 1993. Wetting front instability in uniform soils under low infiltration rates. Master Thesis. New Mexico Institute of Mining and Technology, Socorro, NM.

Appendix 1 Experimental details and predicted finger diameter for diesel experiments

Experiment code	A1	A2	A3	A4	A5	A6	A7	A8
14-20 mil sand	6/23/94	6/24/94	6/21/94	6/21/94	10/27/93	6/23/94	6/23/94	10/21/93
pore size of plate (um)	5	5	5	5	20	5	5	20
temperature (C)	35.0	38.0	31.5	32.5	12.0	34.0	35.0	19.0
viscosity (cSt)	3.73	3.57	3.93	3.87	5.48	3.79	3.73	4.83
surface tension (dyne/cm)	29.0	29.0	29.5	29.0	31.0	29.0	29.0	31.0
saturated conductivity (cm/s)	0.087	0.091	0.082	0.084	0.059	0.086	0.087	0.067
injected volume (cm3)	820	1097	993	762	1682	954	870	1667
average flow rate (cm3/s)	0.41	0.87	0.87	1.06	0.93	1.95	2.01	1.85
system flux (cm/s)	0.0016	0.0034	0.0034	0.0042	0.0037	0.0076	0.0079	0.0073
supplying time (min.)	33.3	21.0	19.0	12.0	30.0	8.2	7.2	15.0
front position (before halting)	3.2	4.3	3.9	3.0	6.6	3.7	3.4	6.5
waiting time bef. slicing (min.)	10.0	10.0	10.0	10.0	10.0	10.0	10.0	20.0
front position (before slicing)	4.2	6.4	6.0	5.5	8.8	8.3	8.2	15.3
transition depth (cm)	N/A	(22-24)	N/A	N/A	N/A	(14-18)	(12-16)	(26?)
finger lasting depth (cm)	29	46	48	49	49	45	45	49
flux ratio	0.019	0.038	0.041	0.050	0.062	0.089	0.091	0.108
normalized size [D*]	N/A	9.77	N/A	N/A	7.11	6.51	6.51	6.09
material constant [Cm]	N/A	1.96	N/A	N/A	1.39	1.24	1.23	1.13
predicted finger size (cm)	2.7	2.7	2.8	2.8	3.0	2.9	2.9	3.2
observed finger size (cm)	N/A	6.0	N/A	N/A	7.0	6.0	6.0	6.0
obs. range of finger size (cm)		4~10			6~8	4~7	3~6	5~8
observed number of fingers	1	(5)~1	1	1	(3)~1	(8)~1	(10)~1	(7)~1
wetting pattern at surface	SD; PD; M	SD; PD; M	PD	PD; M		SD; M	SD; PD; M	

Experiment code	A9	A10	A11	A12	A13	A14	A15	A16
14-20 mil sand	6/20/94	6/22/94	6/22/94	6/22/94	6/17/94	6/20/94	11/22/93	11/30/93
pore size of plate (um)	5	5	5	5	5	5	20	20
temperature (C)	33.0	28.0	28.0	27.0	37.0	33.0	19.0	17.0
viscosity (cSt)	3.84	4.15	4.15	4.22	3.62	3.84	4.83	5.00
surface tension (dyne/cm)	29.0	29.5	29.5	29.5	29.0	29.0	31.0	31.0
saturated conductivity (cm/s)	0.084	0.078	0.078	0.077	0.090	0.084	0.067	0.065
injected volume (cm3)	1004	1000	986	1022	1474	1006	1500	1385
average flow rate (cm3/s)	2.66	2.65	2.79	5.68	7.02	6.71	12.50	15.38
system flux (cm/s)	0.0103	0.0104	0.0109	0.0223	0.0273	0.0261	0.0491	0.0605
supplying time (min.)	6.3	6.3	5.9	3.0	3.5	2.5	2.0	1.5
front position (before halting)	3.9	3.9	3.9	4.0	5.7	3.9	5.9	5.4
waiting time bef. slicing (min.)	10.0	10.0	10.0	6.0	10.0	10.0	10.0	20.0
front position (before slicing)	10.1	10.2	10.4	12.1	22.1	19.5	35.4	78.0
transition depth (cm)	(26)	(24-26)	(22-24)	(14-18)	(36-40)	(18-22)	(12-20)	(13)
finger lasting depth (cm)	47	43	47	44	52	51	46	42
flux ratio	0.122	0.133	0.140	0.290	0.305	0.309	0.731	0.932
normalized size [D*]	6.51	5.34	5.34	4.80	4.89	4.34	4.01	4.06
material constant [Cm]	1.19	0.96	0.96	0.71	0.79	0.63	0.22	0.06
predicted finger size (cm)	3.0	3.1	3.1	3.8	3.8	3.8	10.5	41.3
observed finger size (cm)	6.0	5.0	5.0	4.5	4.5	4.0	4.0	4.0
obs. range of finger size (cm)	4~8	4~6	3~5	3~5	2~6	3~6	3~5	3~5
observed number of fingers	(6)~1	(11)~4	(8)~1	(17)~1	(11)~(7)	(14)~3	(16)~9	>10
wetting pattern at surface	M	SD; PD; M	SD; M	SD; PD; M	SD; PD; M	SD; PD; M		

Abbreviation: spotty dry: SD; partially dry: PD; mount: M; number within ( ) meaning finger overlaped; number with underline means finger reached the bottom base

Appendix 1 Continued

Experiment code	B1	B2	B3	B4	B5	B6	B7	B8
20-30 mil sand	6/27/94	10/26/93	10/11/93	10/6/93	10/4/93	6/27/94	6/28/94	6/16/94
pore size of plate (um)	5	20	20	20	20	5	5	5
temperature (C)	39.0	15.5	25.5	29.5	30.0	40.0	37.0	37.0
viscosity (cSt)	3.52	5.13	4.33	4.06	4.03	3.47	3.62	3.62
surface tension (dyne/cm)	29.0	31.0	30.0	29.5	29.5	29.0	29.0	29.0
saturated conductivity (cm/s)	0.056	0.038	0.045	0.048	0.049	0.057	0.054	0.054
injected volume (cm3)	1136	1818	1094	1470	2570	1149	981	753
average flow rate (cm3/s)	0.79	1.01	1.22	1.50	1.71	2.55	2.72	5.02
system flux (cm/s)	0.0031	0.0040	0.0048	0.0059	0.0067	0.0099	0.0106	0.0195
supplying time (min.)	24.0	30.0	15.0	16.3	25.0	7.5	6.0	2.5
front position (before halting)	4.4	7.1	4.3	5.8	10.1	4.5	3.8	2.9
waiting time bef. slicing (min.)	10.0	10.0	30.0	30.0	0.0	10.0	10.0	40.0
front position (before slicing)	6.3	9.5	12.9	16.4	10.1	10.4	10.2	49.7
transition depth (cm)	N/A	(20-26)	N/A	N/A	N/A	N/A	N/A	(14-18)
finger lasting depth (cm)	26	42	36	38	27	47	39	47
flux ratio	0.055	0.104	0.105	0.122	0.138	0.176	0.196	0.360
normalized size [D*]	5.28	4.94	5.84	5.19	N/A	4.53	N/A	4.53
material constant [Cm]	1.04	0.92	1.09	0.95	N/A	0.78	N/A	0.60
predicted finger size (cm)	3.2	3.6	3.5	3.5	3.6	3.7	3.8	4.8
observed finger size (cm)	7.0	7.0	8.0	7.0	N/A	6.0	N/A	6.0
obs. range of finger size (cm)	4~11	4~10	4~11	5.5~10		5~9		5~8
observed number of fingers	(3)~1	(3)~1	(4)~1	(4)~1	1	(5)~1	1	(6)~1
wetting pattern at surface	SD; PD; M					SD; M	SD; M	M

Experiment code	B9	B10	B11	B12	B13	B14	B15
20-30 mil sand	11/1/93	6/16/94	6/17/94	4/19/94	4/12/94	11/29/93	12/1/93
pore size of plate (um)	20	5	5	20	20	20	5
temperature (C)	20.0	37.0	35.0	26.5	19.0	16.5	15.5
viscosity (cSt)	4.74	3.62	3.73	4.26	4.83	5.04	5.13
surface tension (dyne/cm)	31.0	29.0	29.0	29.5	31.0	31.0	31.0
saturated conductivity (cm/s)	0.041	0.054	0.053	0.046	0.041	0.039	0.038
injected volume (cm3)	1364	1481	1478	1227	1142	1500	1500
average flow rate (cm3/s)	4.55	7.05	7.70	8.18	11.42	12.50	16.67
system flux (cm/s)	0.0179	0.0274	0.0299	0.0321	0.0449	0.0491	0.0655
supplying time (min.)	5.0	3.5	3.2	2.5	1.67	2.0	1.5
front position (before halting)	5.4	5.8	5.7	4.8	4.5	5.9	5.9
waiting time bef. slicing (min.)	20.0	10.0	10.0	15.0	22.0	10.0	20.0
front position (before slicing)	26.8	22.2	23.7	33.7	63.7	35.4	84.5
transition depth (cm)	(12)	(24)	(22)	12	12	16	N/A
finger lasting depth (cm)	43	50	47	41	43	46	43
flux ratio	0.432	0.506	0.569	0.698	1.105	1.264	1.716
normalized size [D*]	2.82	4.53	4.53	4.08	3.53	4.24	N/A
material constant [Cm]	0.33	0.47	0.41	0.26	N/A	N/A	N/A
predicted finger size (cm)	5.7	6.2	7.1	10.3	N/A	N/A	N/A
observed finger size (cm)	4.0	6.0	6.0	5.5	5.0	6.0	N/A
obs. range of finger size (cm)	3~5	5~8	3~9	3~7	3~5.5	4~7	
observed number of fingers	15~9	(6)~(3)	(7)~(3)	(8)~1	(9)~5	(9)~(2)	1
wetting pattern at surface		M	SD; PD; M	M	M		

Appendix 1 Continued

Experiment code	C1	C2	C3	C4	C5	C6	C7	C8	C9
30-40 mil sand	10/5/93	9/29/93	10/20/93	10/12/93	11/7/93	4/5/94	3/31/94	4/7/94	3/29/94
pore size of plate (um)	20	20	20	20	20	20	20	20	5
temperature (C)	31.0	28.0	19.0	25.5	18.0	21.5	16.0	22.0	13.0
viscosity (cSt)	3.96	4.15	4.83	4.33	4.91	4.62	5.09	4.58	5.37
surface tension (dyne/cm)	29.5	29.5	31.0	30.0	31.0	31.0	31.0	29.5	31.0
saturated conductivity (cm/s)	0.032	0.031	0.026	0.029	0.026	0.028	0.025	0.028	0.024
injected volume (cm3)	2832	4111	1710	984	1500	1703	1414	1183	1601
average flow rate (cm3/s)	1.600	1.713	1.900	3.279	4.167	4.730	4.714	6.570	6.670
system flux (cm/s)	0.0063	0.0067	0.0075	0.0129	0.0164	0.0186	0.0185	0.0258	0.0262
supplying time (min.)	29.5	40.0	15.0	5.0	6.0	6.0	5.0	3.0	4.0
front position (before halting)	11.1	16.2	6.7	3.9	5.9	6.7	5.6	4.6	6.3
waiting time bef. slicing (min.)	20.0	0.0	20.0	30.0	40.0	25.0	23.0	22.0	25.0
front position (before slicing)	18.7	16.2	15.7	27.1	45.2	34.6	31.1	38.7	45.6
transition depth (cm)	N/A	N/A	(12)	(0)	(18)	(9)	(14)	8	N/A
finger lasting depth (cm)	44	45	43	44	47	42	35	32	43
flux ratio	0.196	0.219	0.283	0.437	0.631	0.674	0.740	0.929	1.106
normalized size [D*]	N/A	N/A	3.95	3.77	3.45	3.45	3.45	3.11	3.95
material constant [Cm]	N/A	N/A	0.59	0.44	0.27	0.23	0.19	0.05	N/A
predicted finger size (cm)	4.1	4.3	4.9	6.0	9.5	10.7	13.4	46.7	N/A
observed finger size (cm)	N/A	N/A	8.0	7.4	7.0	7.0	7.0	6.0	8
obs. range of finger size (cm)			6~11	5~8	4~8	5.5~10	5~9	5~8	7~10
observed number of fingers	(2)	(2)	(5)~(3)	(6)~1	(8)~1	(3)~1	(4)~1	(7)~1	(2)
wetting pattern at surface	PD	SD; PD; M		PD		PD	PD	M	M

Experiment code	D1	D2	D3	D4	D5	D6	D7
40-60 mil sand	11/10/93	9/28/93	11/9/93	9/25/93	2/15/94	2/28/94	11/8/93
pore size of plate (um)	20	5	20	5	20	20	20
temperature (C)	18.0	31.0	19.0	26.5	13.0	16.0	25.5
viscosity (cSt)	4.91	3.96	4.83	4.26	5.37	5.09	4.33
surface tension (dyne/cm)	31.0	29.5	31.0	30.0	31.0	31.0	30.0
saturated conductivity (cm/s)	0.014	0.017	0.014	0.016	0.013	0.013	0.016
injected volume (cm3)	878	4234	1401	3175	2769	3625	1243
average flow rate (cm3/s)	0.244	1.764	1.460	1.764	1.538	2.014	2.959
system flux (cm/s)	0.0010	0.0069	0.0057	0.0069	0.0060	0.0079	0.0116
supplying time (min.)	60.0	40.0	16.0	30.0	30.0	30.0	7.0
front position (before halting)	3.5	16.6	5.5	12.4	10.9	14.2	4.9
waiting time bef. slicing (min.)	15.0	20.0	20.0	0.0	10.0	20.0	10.0
front position (before slicing)	4.3	24.8	12.4	12.4	14.5	23.7	11.9
transition depth (cm)	N/A	N/A	N/A	N/A	N/A	N/A	N/A
finger lasting depth (cm)	24	25	26	21	26	37	22
flux ratio	0.069	0.398	0.403	0.427	0.473	0.586	0.732
normalized size [D*]	N/A	N/A	N/A	N/A	N/A	N/A	N/A
predicted finger size (cm)	5.2	7.6	8.1	8.2	9.2	11.7	17.4
observed finger size (cm)	N/A	N/A	N/A	N/A	N/A	N/A	N/A
obs. range of finger size (cm)							
observed number of fingers	1	1	1	1	1	(2)	1
wetting pattern at surface					M	M	

Appendix 2 Experimental details and predicted finger diameter for water control experiments

Experiment code	W1	W2	W3	W4	W5	W6	W7
14-20 mil sand	11/4/94	11/3/94	10/28/94	10/13/94	10/31/94	11/10/94	11/1/94
pore size of plate (um)	5	5	5	5	5	5	5
temperature (C)	16.0	19.0	19.0	19.0	18.0	18.0	16.0
viscosity (cSt)	1.00	1.00	1.00	1.00	1.00	1.00	1.00
surface tension (dyne/cm)	72.0	72.0	72.0	72.0	72.0	72.0	72.0
saturated conductivity (cm/s)	0.324	0.324	0.324	0.324	0.324	0.324	0.324
injected volume (cm3)	509	520	759	774	502	548	499
average flow rate (cm3/s)	0.565	2.167	6.324	6.453	12.446	13.333	24.953
system flux (cm/s)	0.0044	0.0085	0.0249	0.0254	0.0489	0.0524	0.0981
supplying time (min.)	15.0	4.0	2.0	2.0	0.7	0.7	0.3
front position (before halting)	4.0	2.0	3.0	3.0	2.0	2.2	2.0
waiting time bef. slicing (min.)	5.0	5.0	10.0	10.0	10.0	5.0	5.0
front position (before slicing)	5.3	4.6	17.9	18.3	31.3	17.9	31.4
transition depth (cm)	(6)	(6)	(6)	(6)	(6)	(6)	(6)
finger lasting depth (cm)	50	52	47	44	50	52	52
flux ratio	0.014	0.026	0.077	0.078	0.151	0.162	0.302
normalized size [D*]	2.52	2.32	2.21	2.32	2.42	2.21	2.16
material constant [Cm]	0.52	0.47	0.43	0.44	0.43	0.39	0.31
predicted finger size (cm)	5.6	5.7	6.0	6.0	6.6	6.6	8.0
observed finger size (cm)	4.9	4.5	4.3	4.5	4.7	4.3	4.2
obs. range of finger size (cm)	3.5~6.5	3.5~5	3.5~5	3.5~5.5	3.5~5.5	3.5~6.5	3.5~5.5
observed number of fingers	(8)~2	(11)~2	(11)~5	(13)~(3)	(9)~3	(11)~2	(13)~2
wetting pattern at surface	SD; PD	SD; PD		SD; PD; M	SD; M	SD; PD	SD; M

Appendix 3a: Typical diesel experiments for 14-20 sand; flux ratio at 0.09; experiment code: A7.

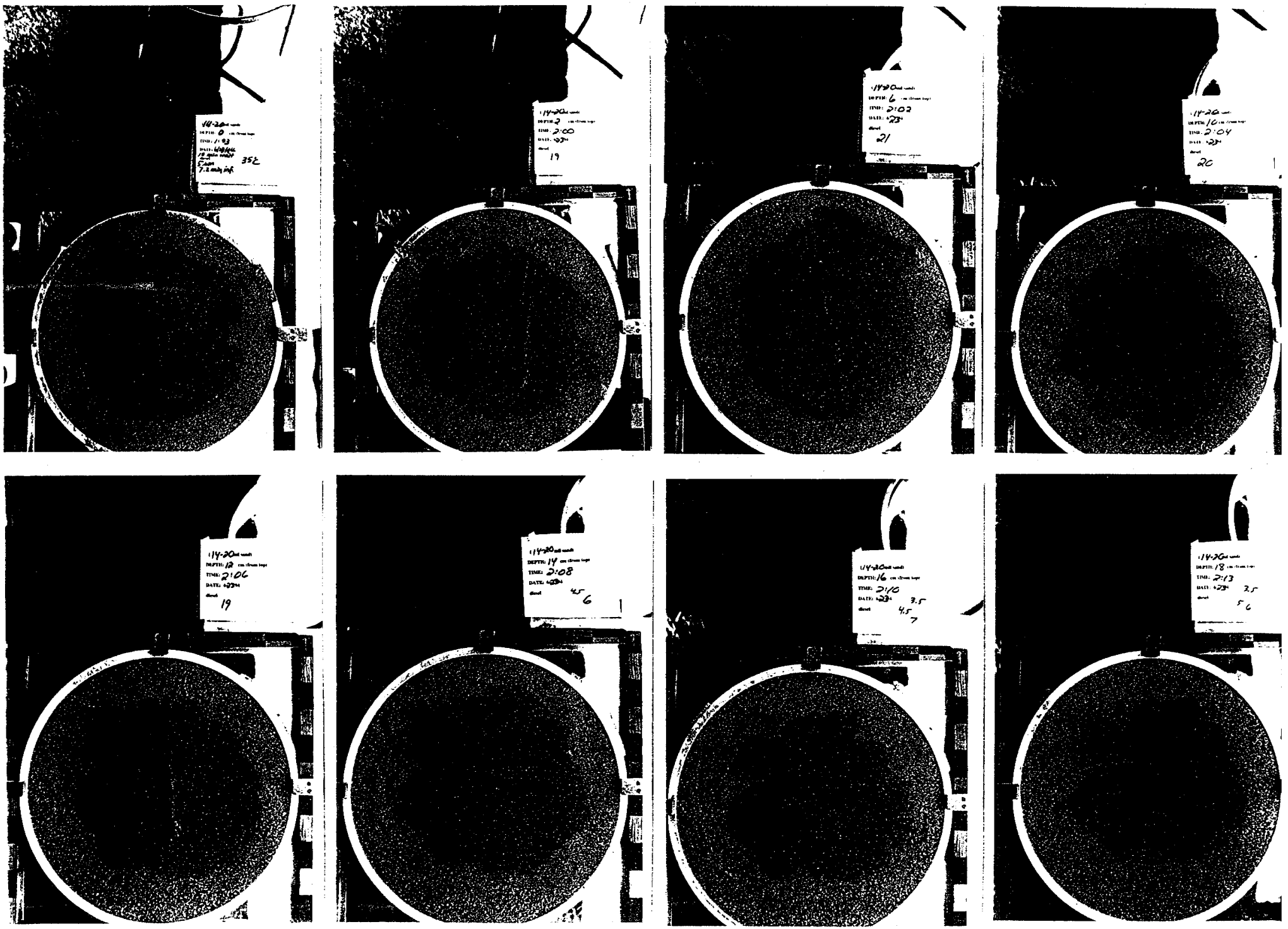

Appendix 3a continued

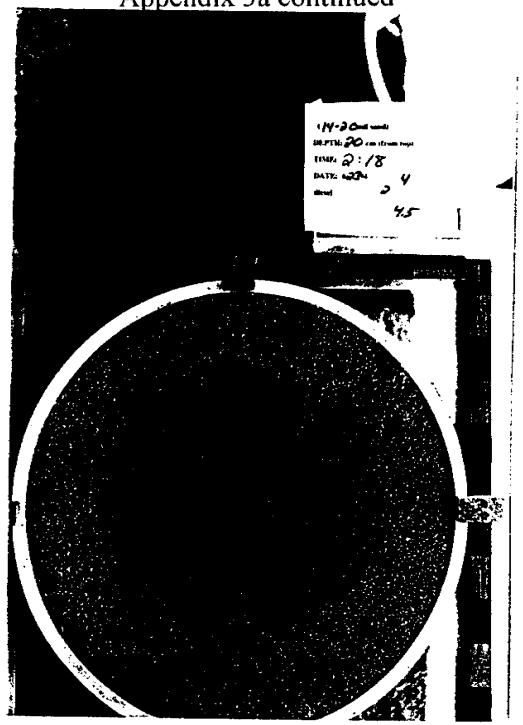

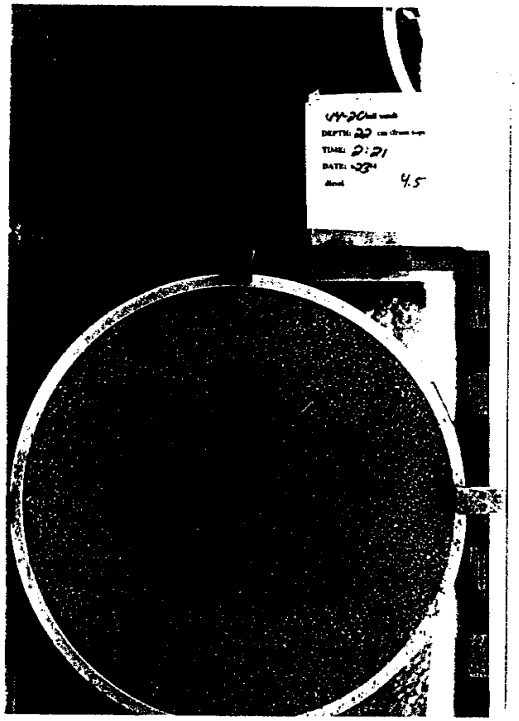

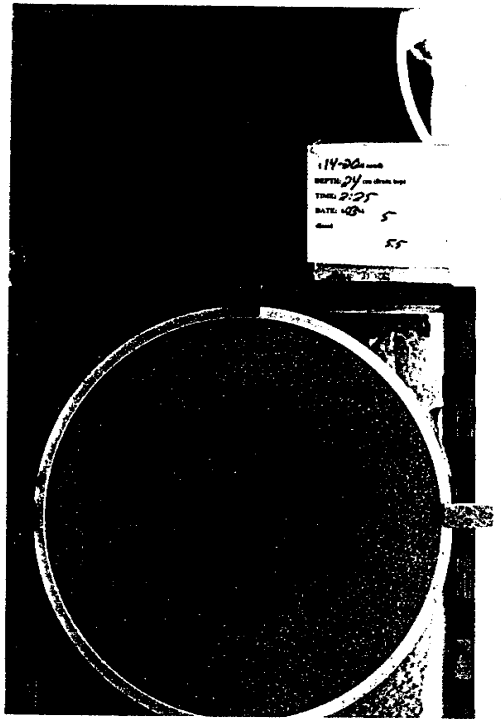

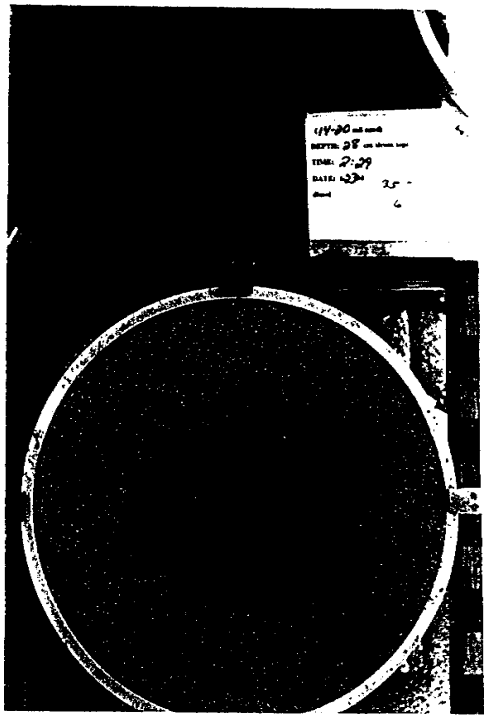

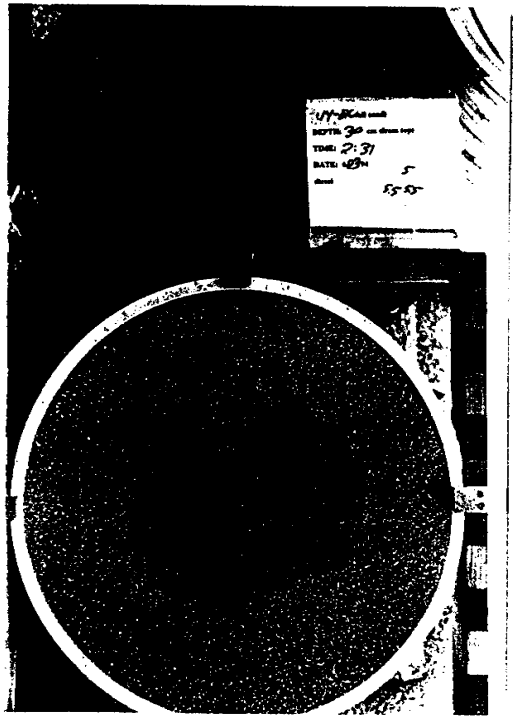

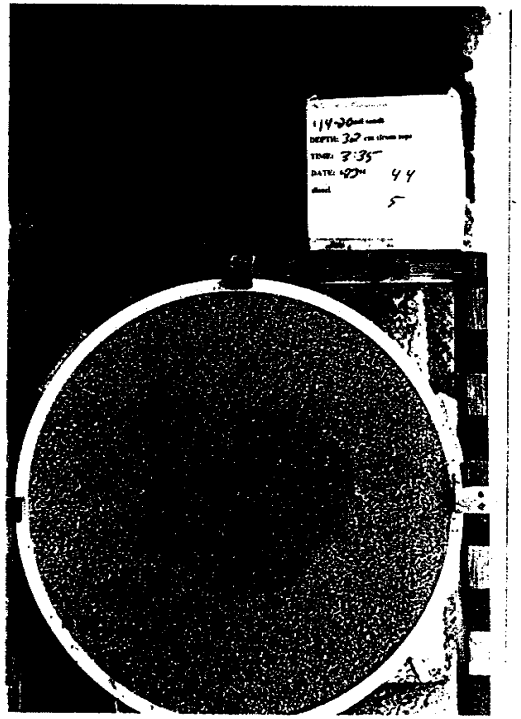

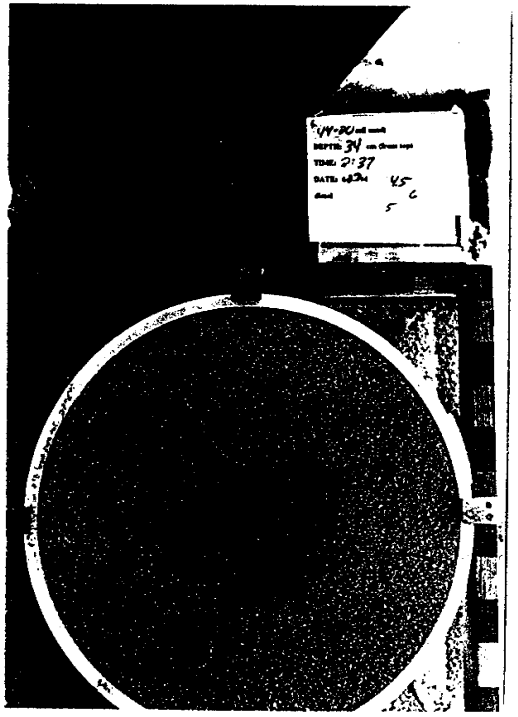

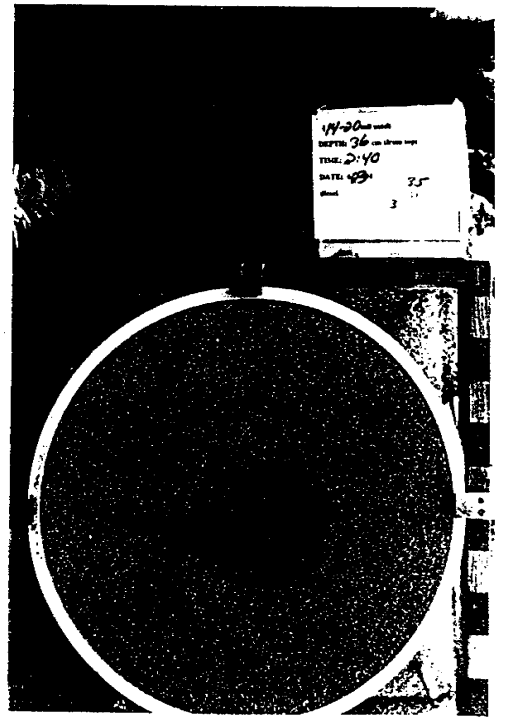

Appendix 3a continued

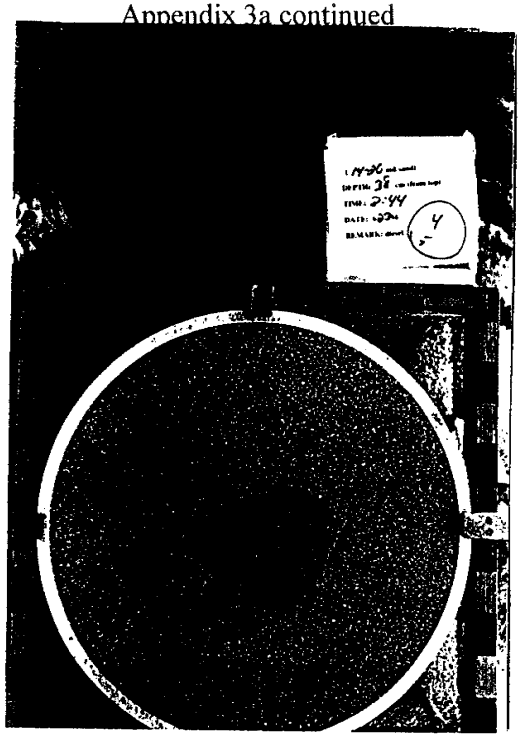

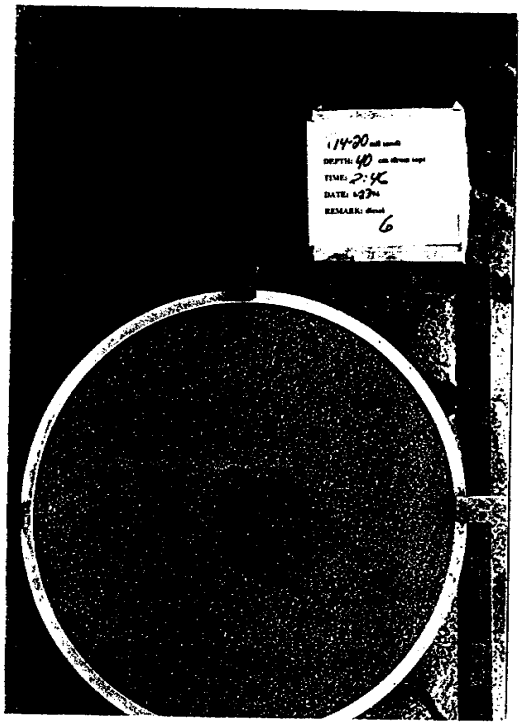

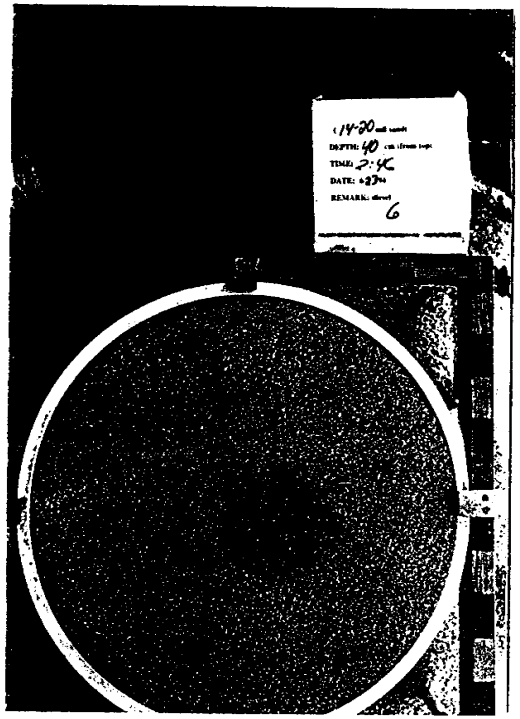

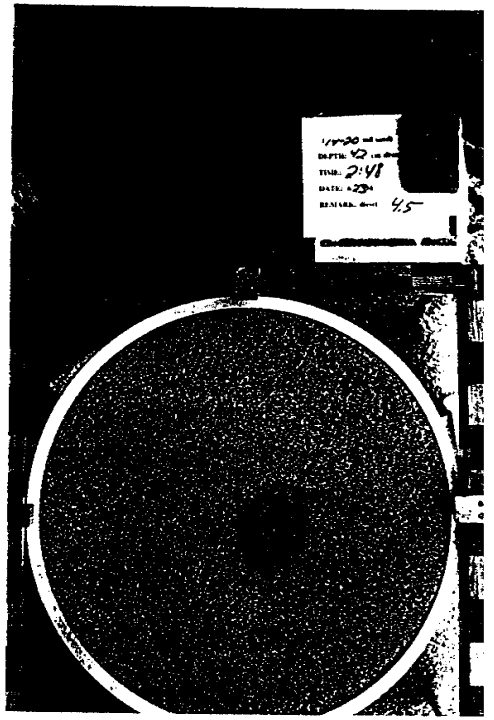

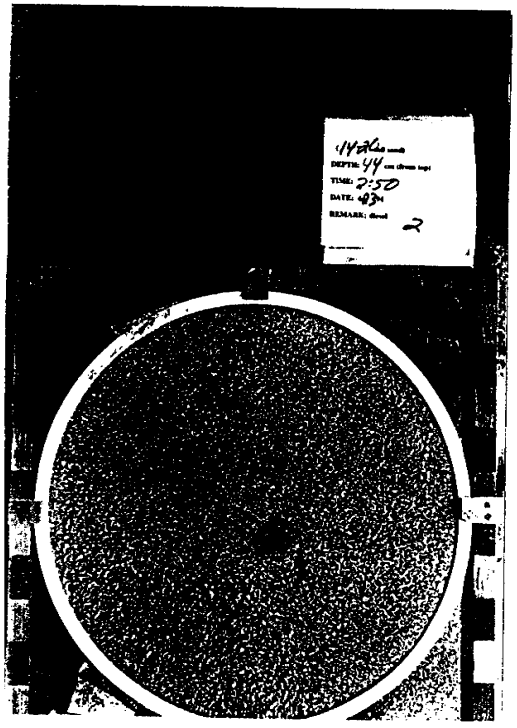

Appendix 3b: Typical diesel experiments for 14-20 sand; flux ratio at 0.29; experiment code: A12.

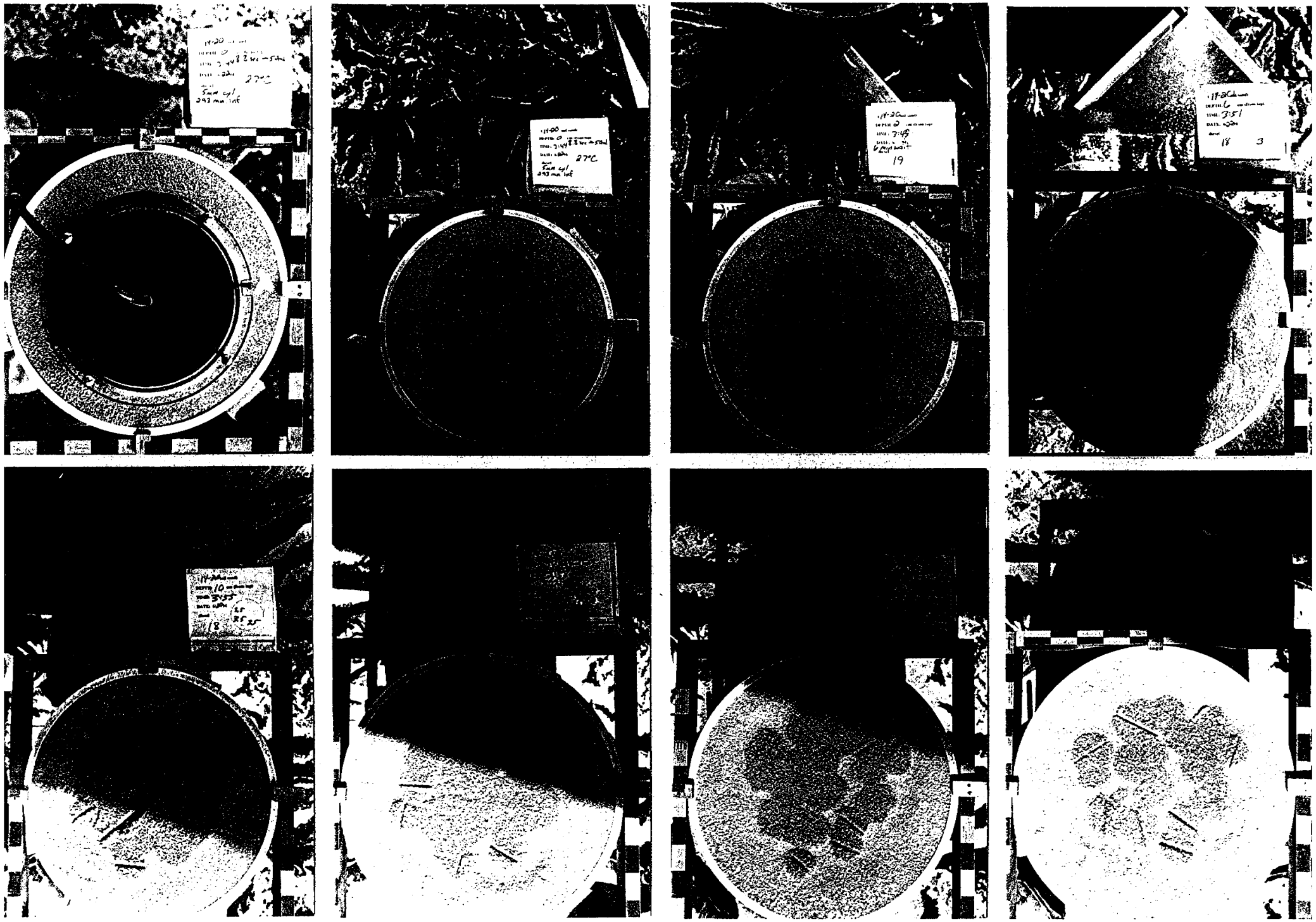

Appendix 3b continued

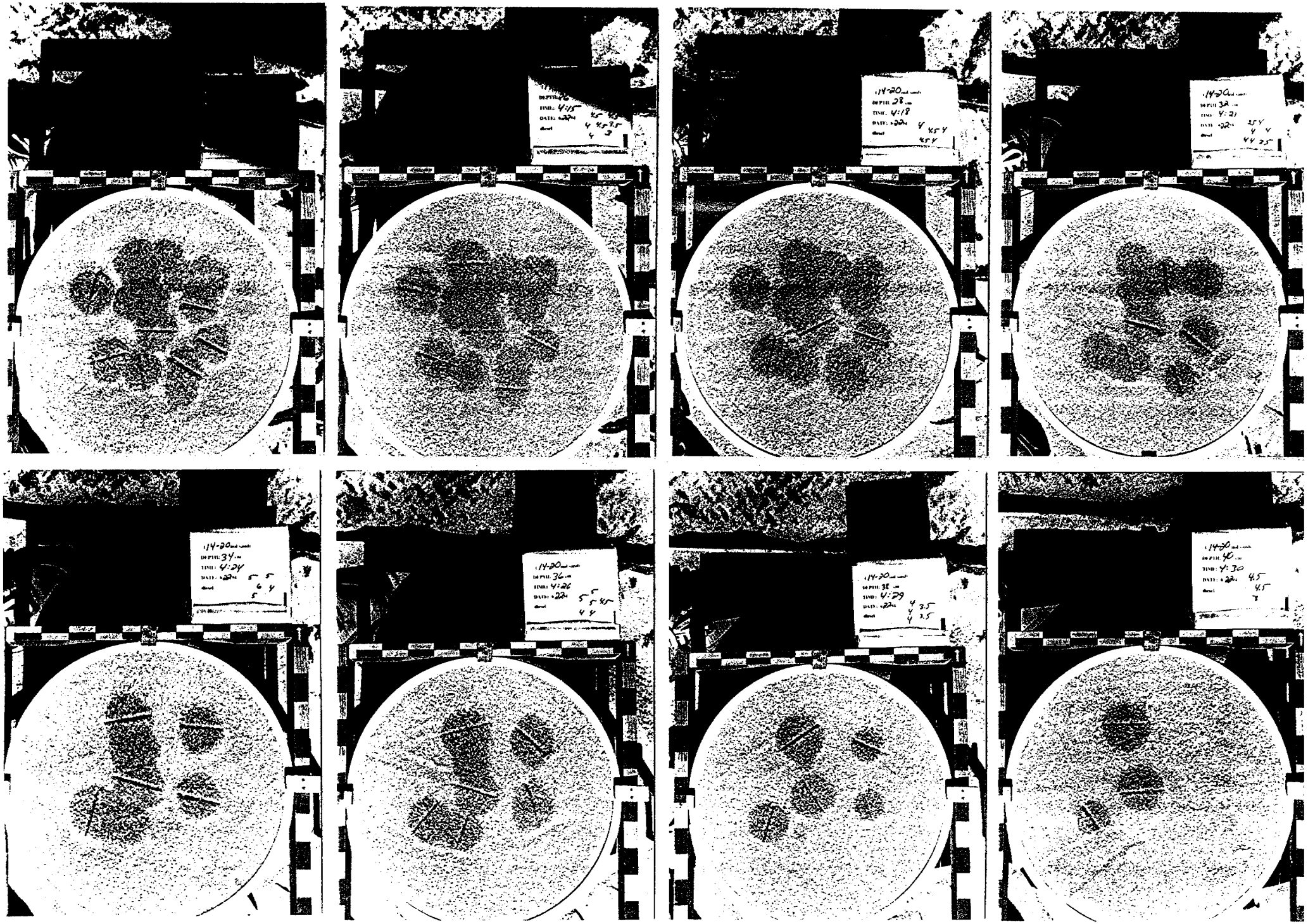

Appendix 4a: Typical diesel experiments for 20-30 sand; flux ratio at 0.1; experiment code: B2.

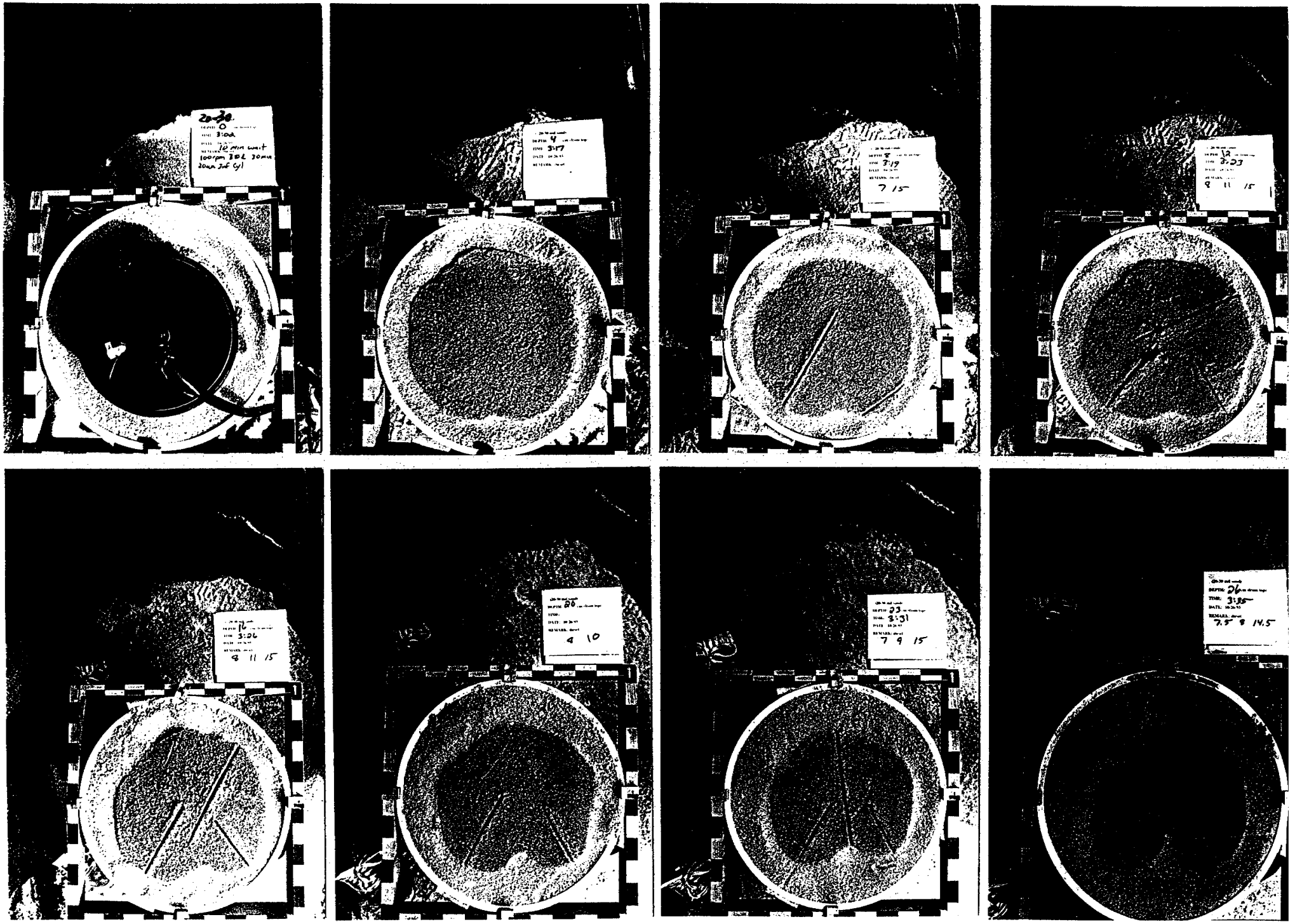

Appendix 4a continued

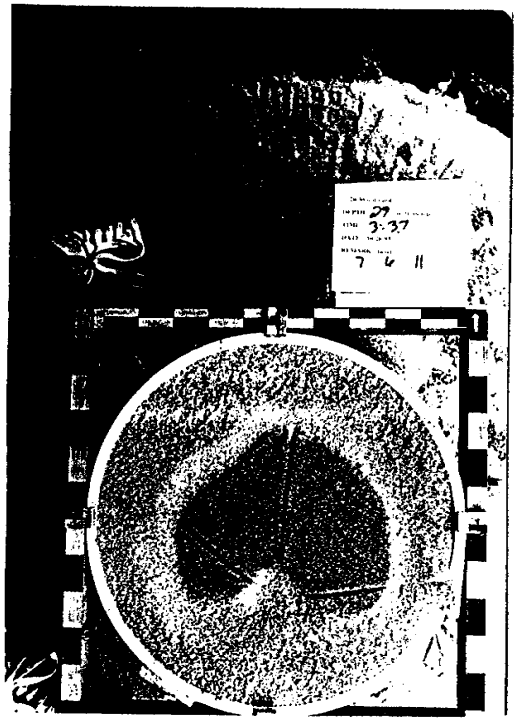

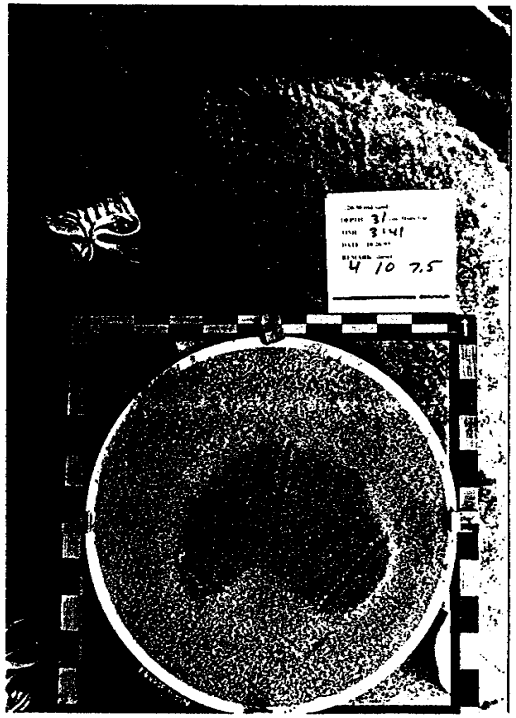

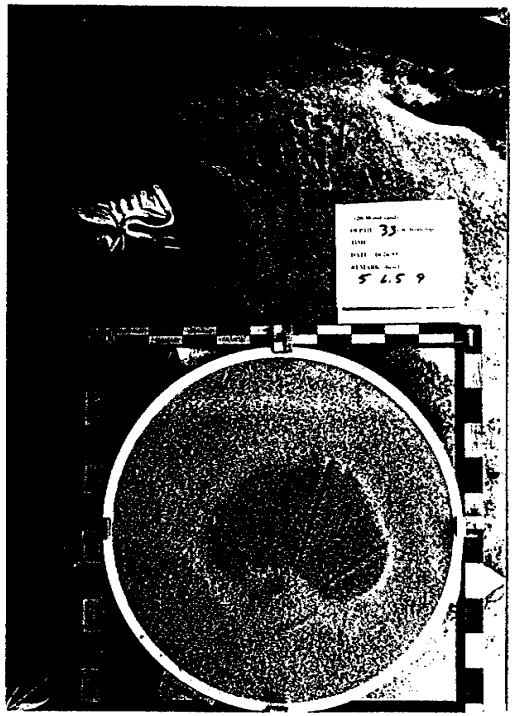

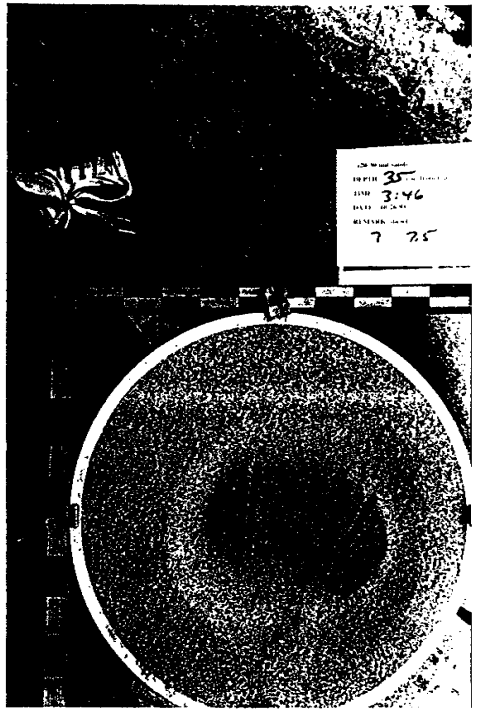

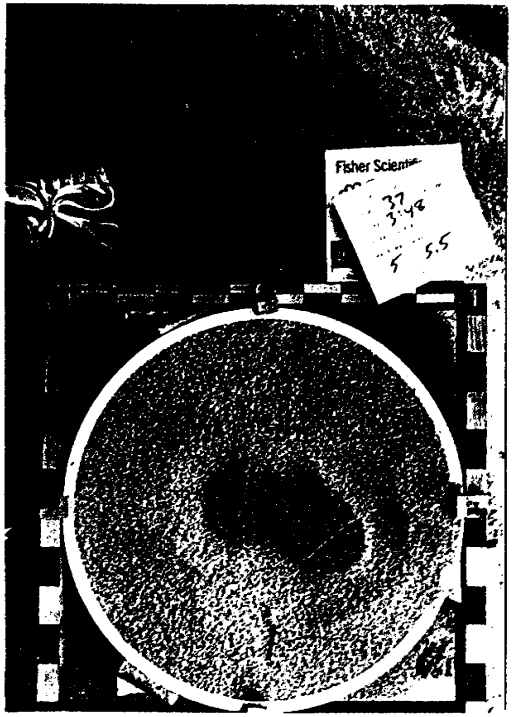

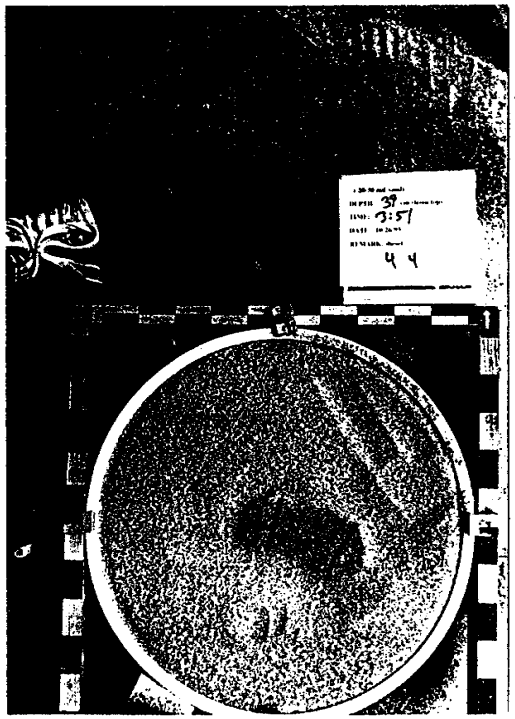

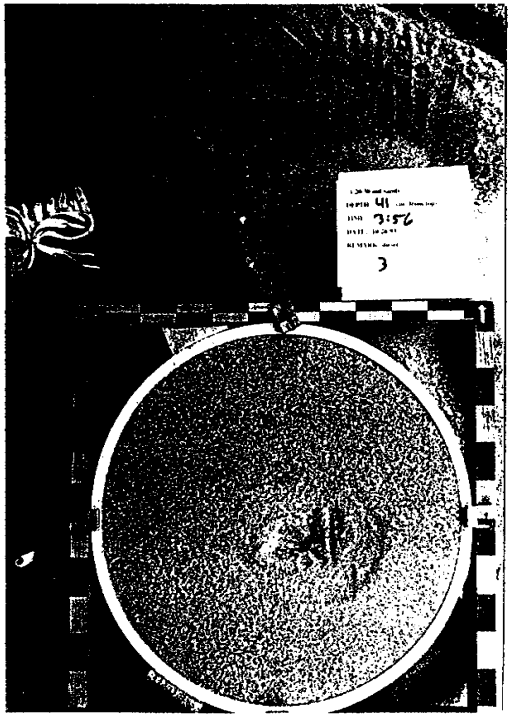

Appendix 4b: Typical diesel experiments for 20-30 sand; flux ratio at 1.1; experiment code: B13.

Appendix 4b: Typical diesel experiments for 20-30 sand; flux ratio at 1.1; experiment code: B13.

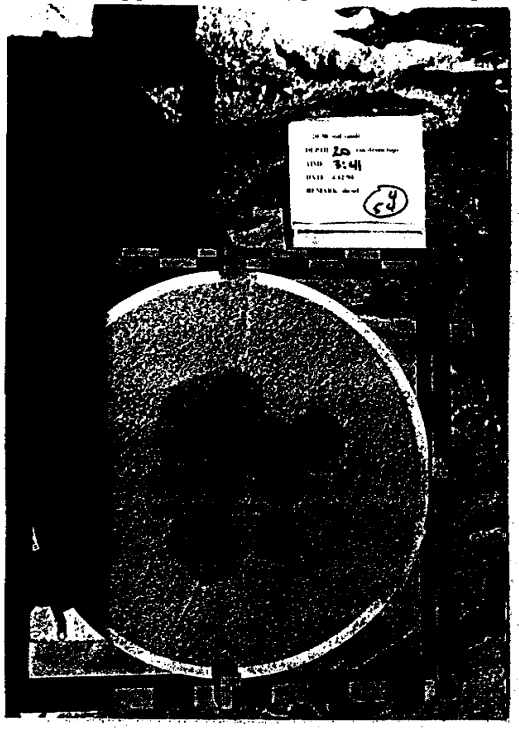


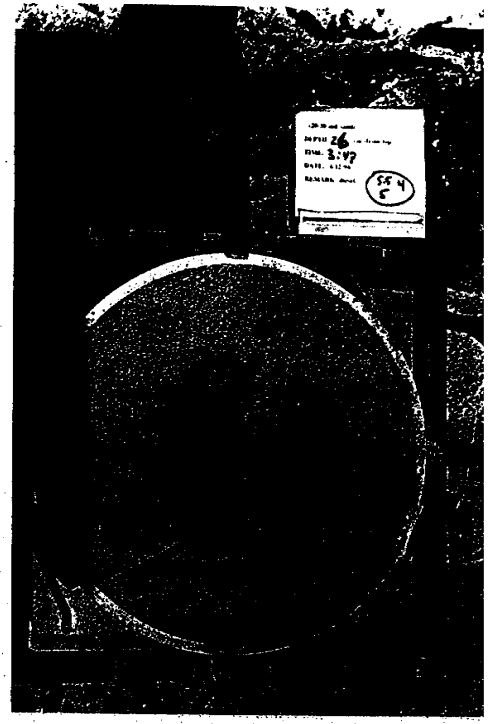

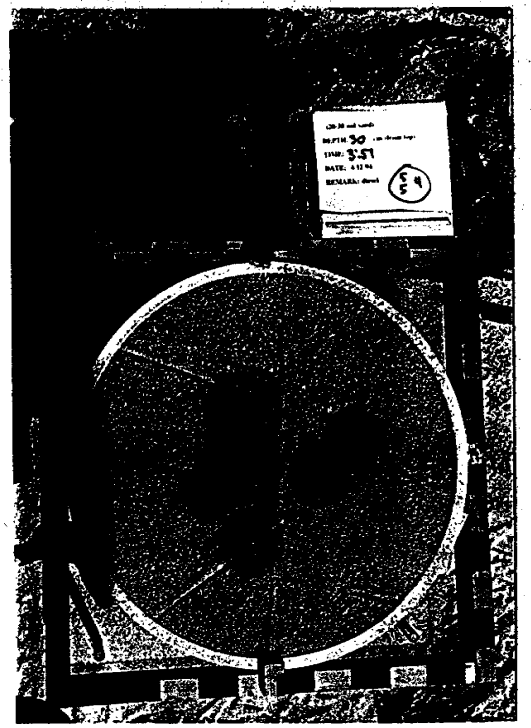
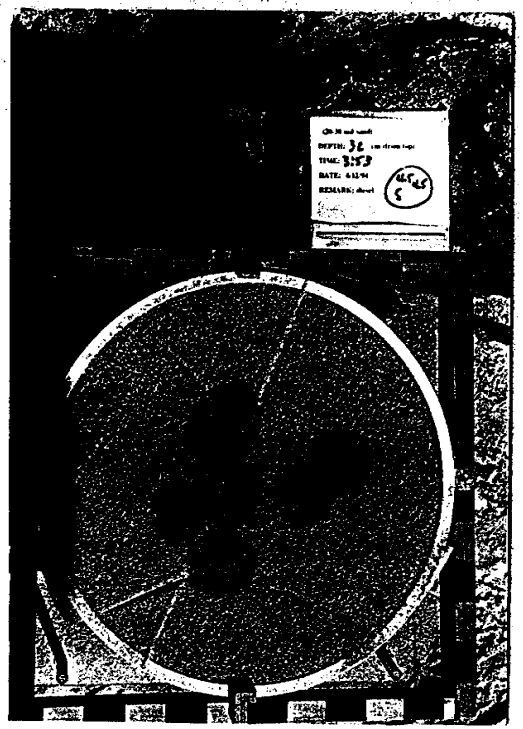
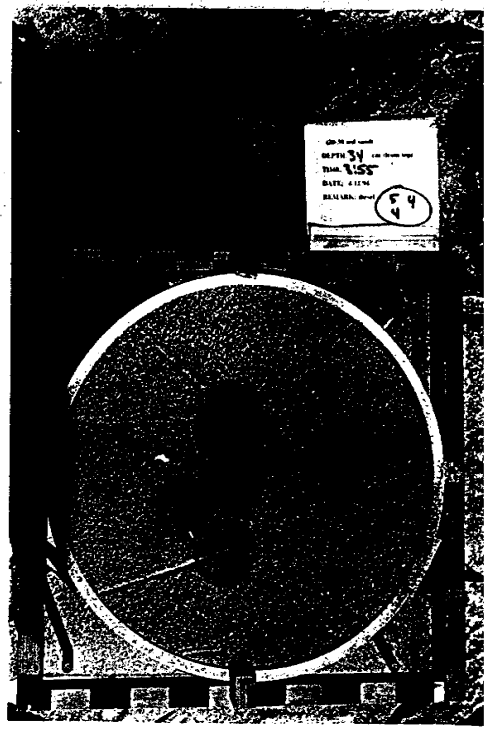

Appendix 4b continued

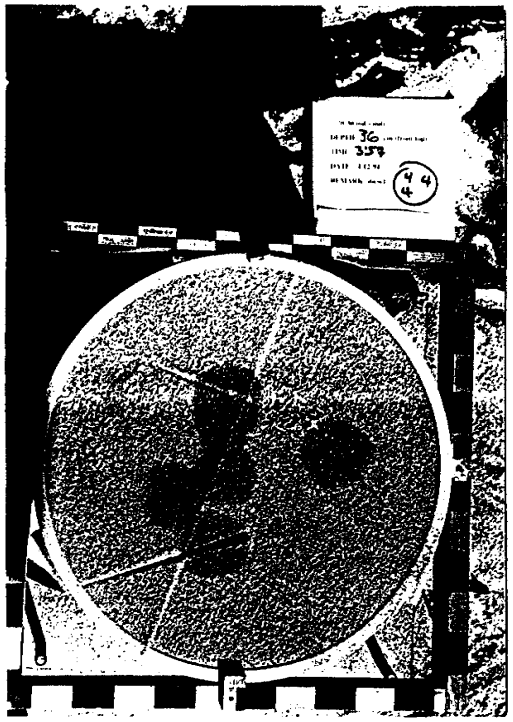

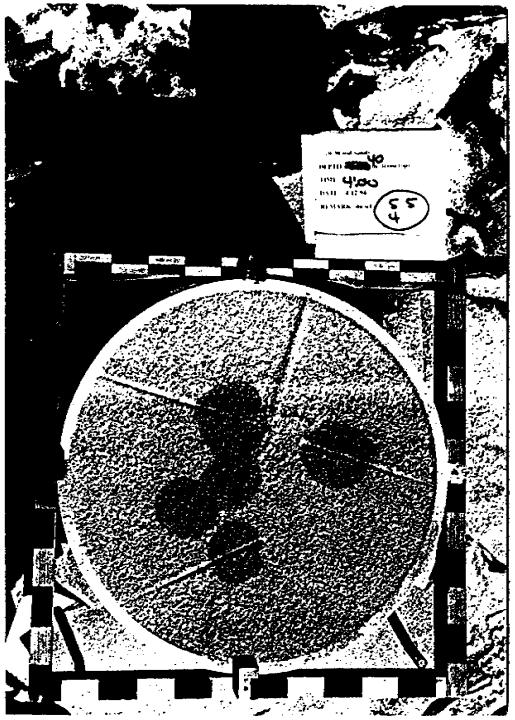
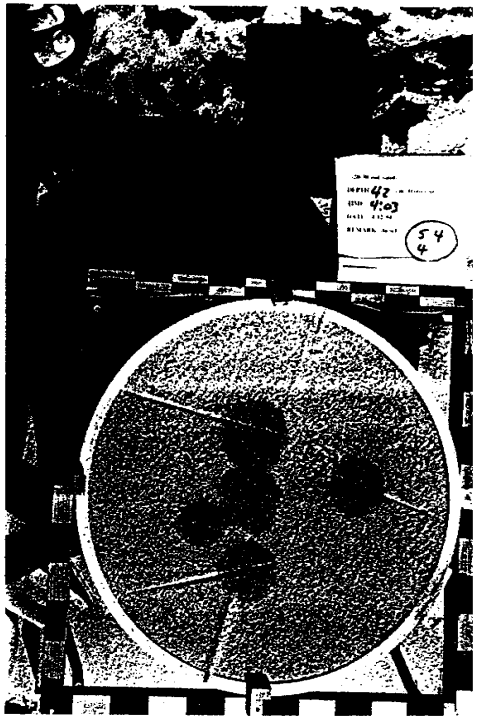

Appendix 5a: Typical diesel experiments for 30-40 sand; flux ratio at 0.23; experiment code: C3.

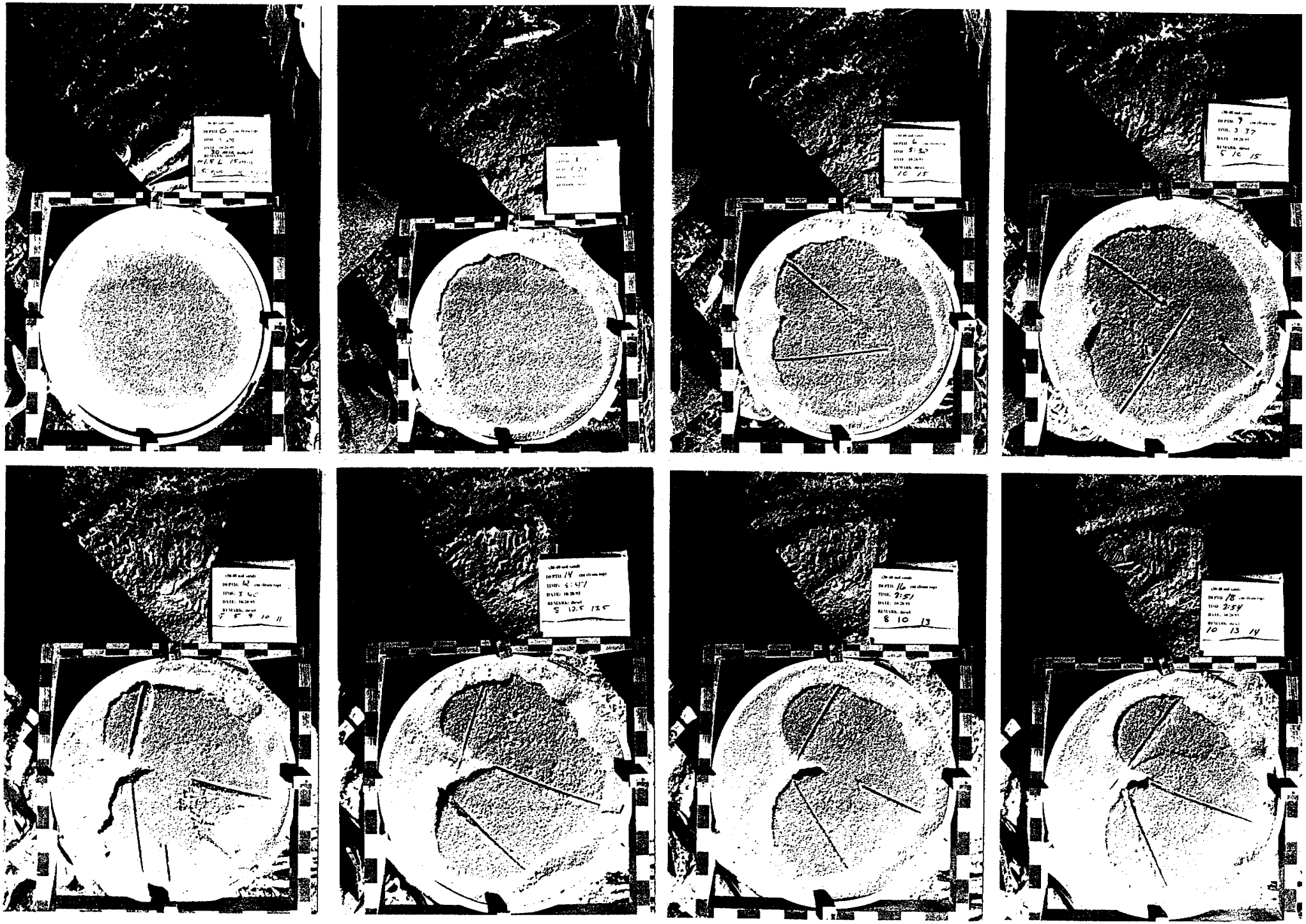

Appendix 5a continued

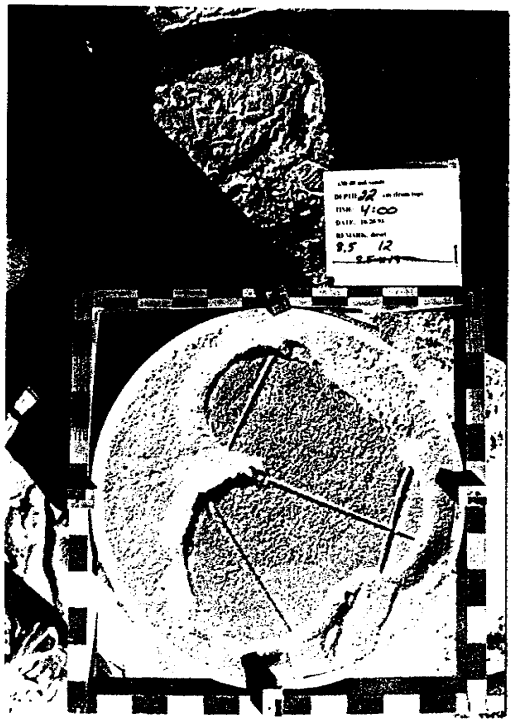

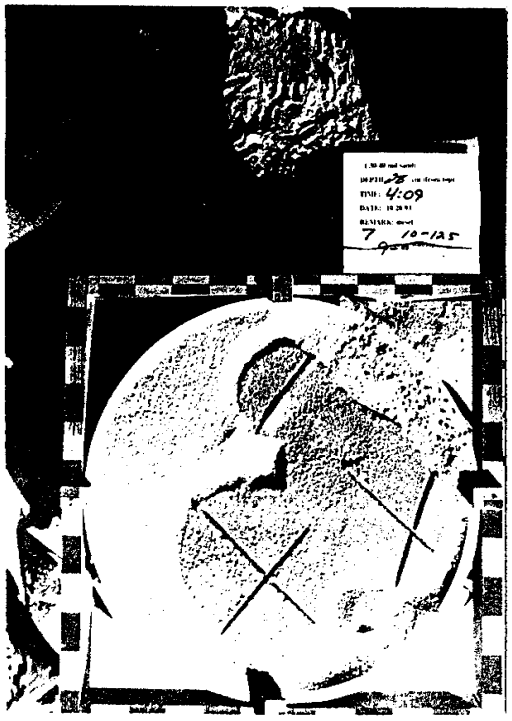

Appendix 5a continued

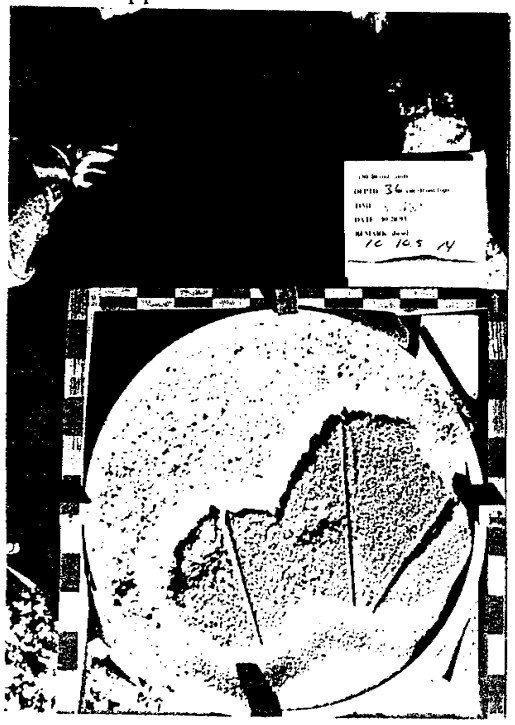

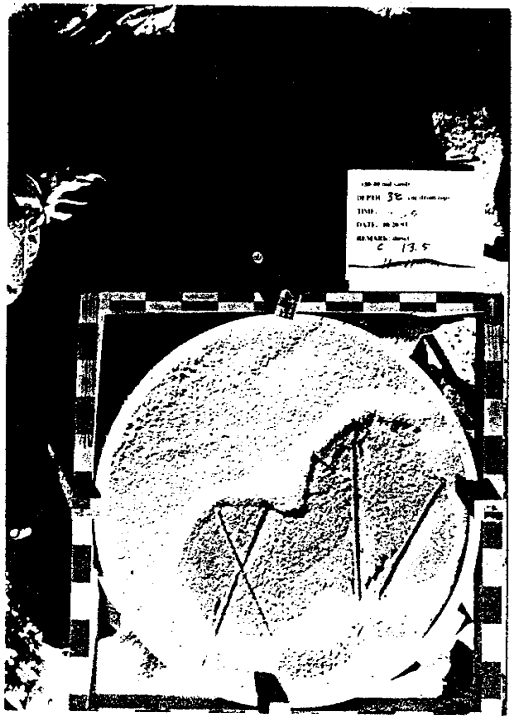

Appendix 5b: Typical diesel experiments for 30-40 sand; flux ratio at 0.68; experiment code: C5.

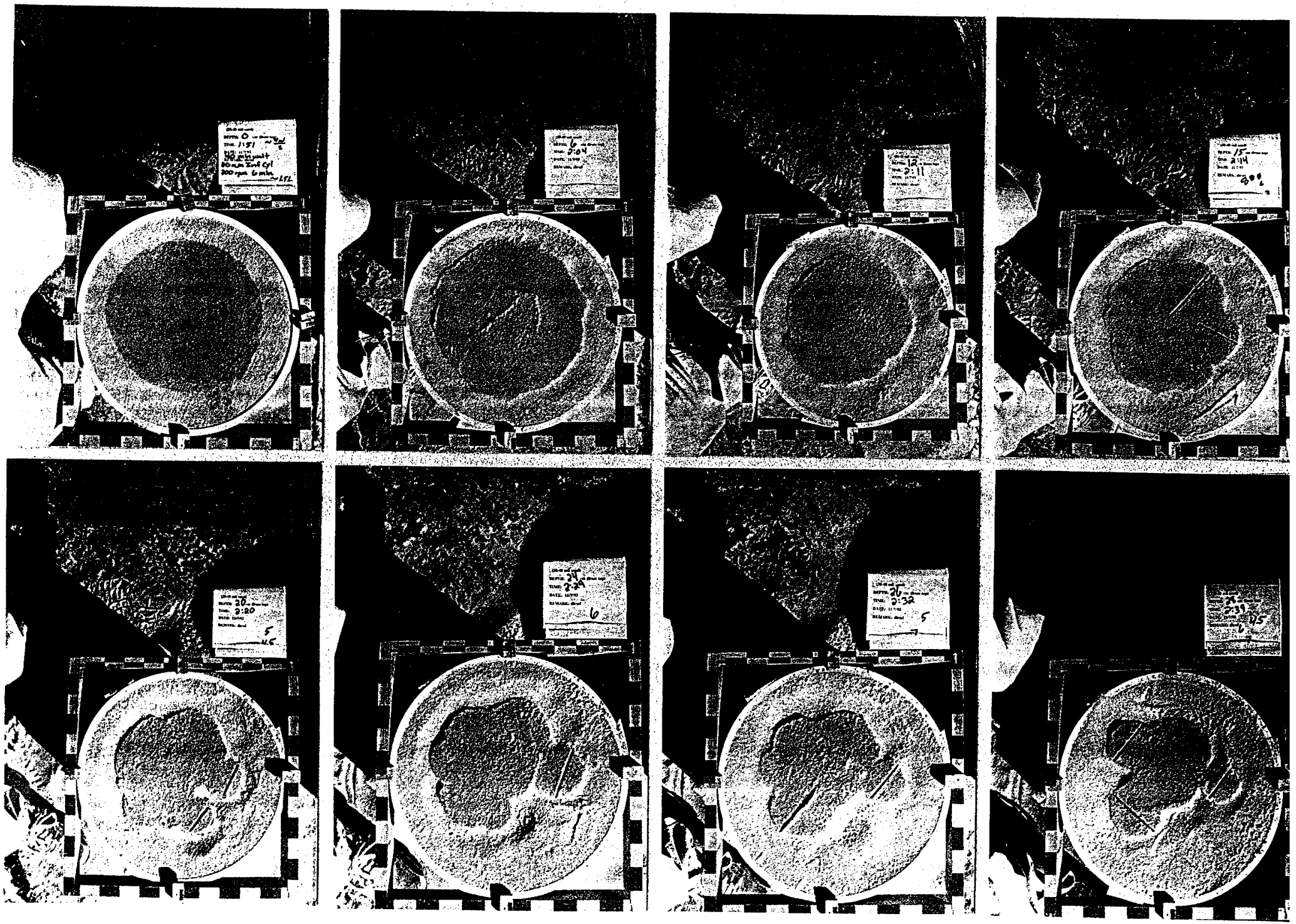

Appendix 5b continued

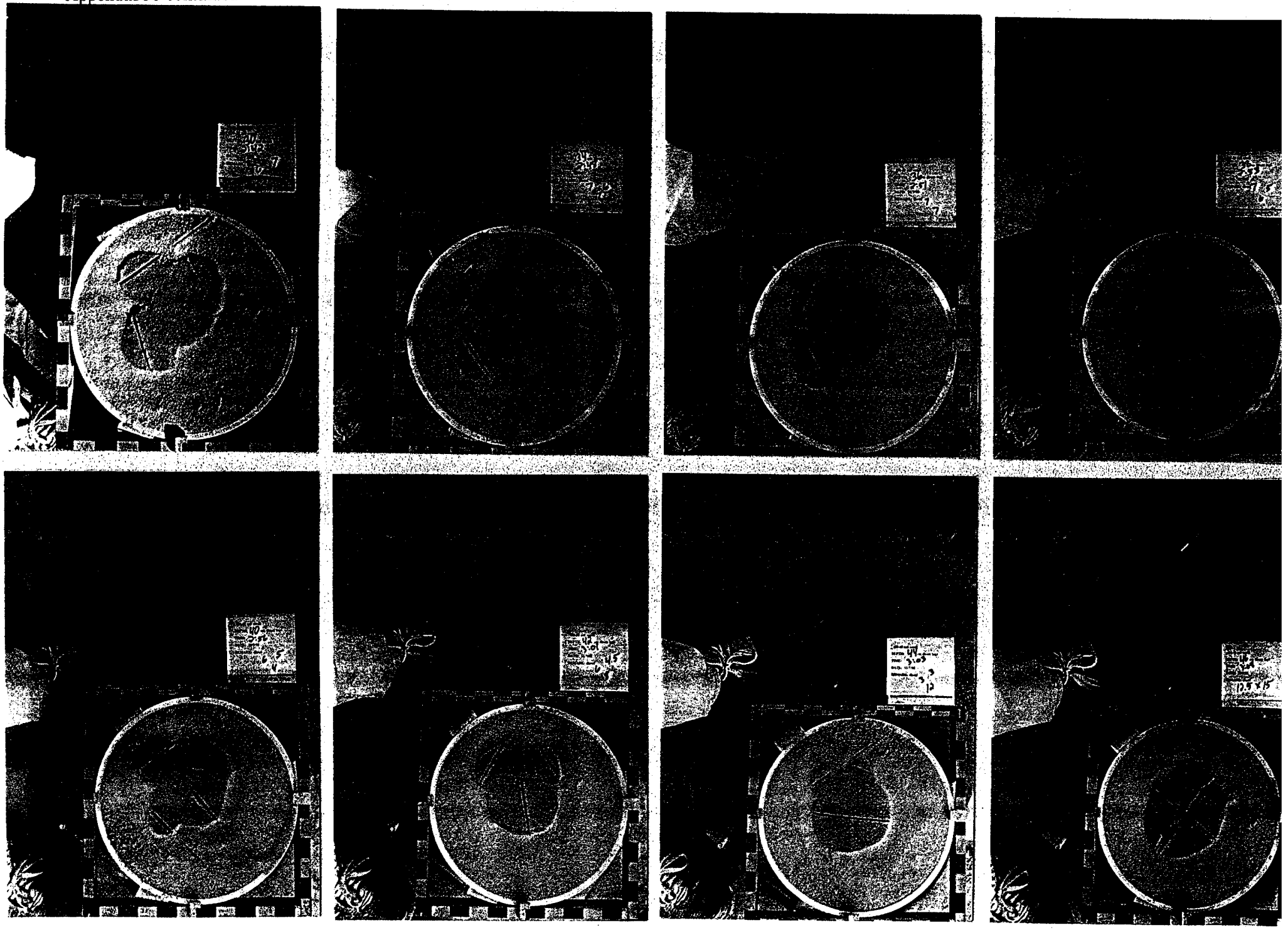

Appendix 6: A typical result for the water control experiment; flux ratio at 0.3; experiment code: W7.

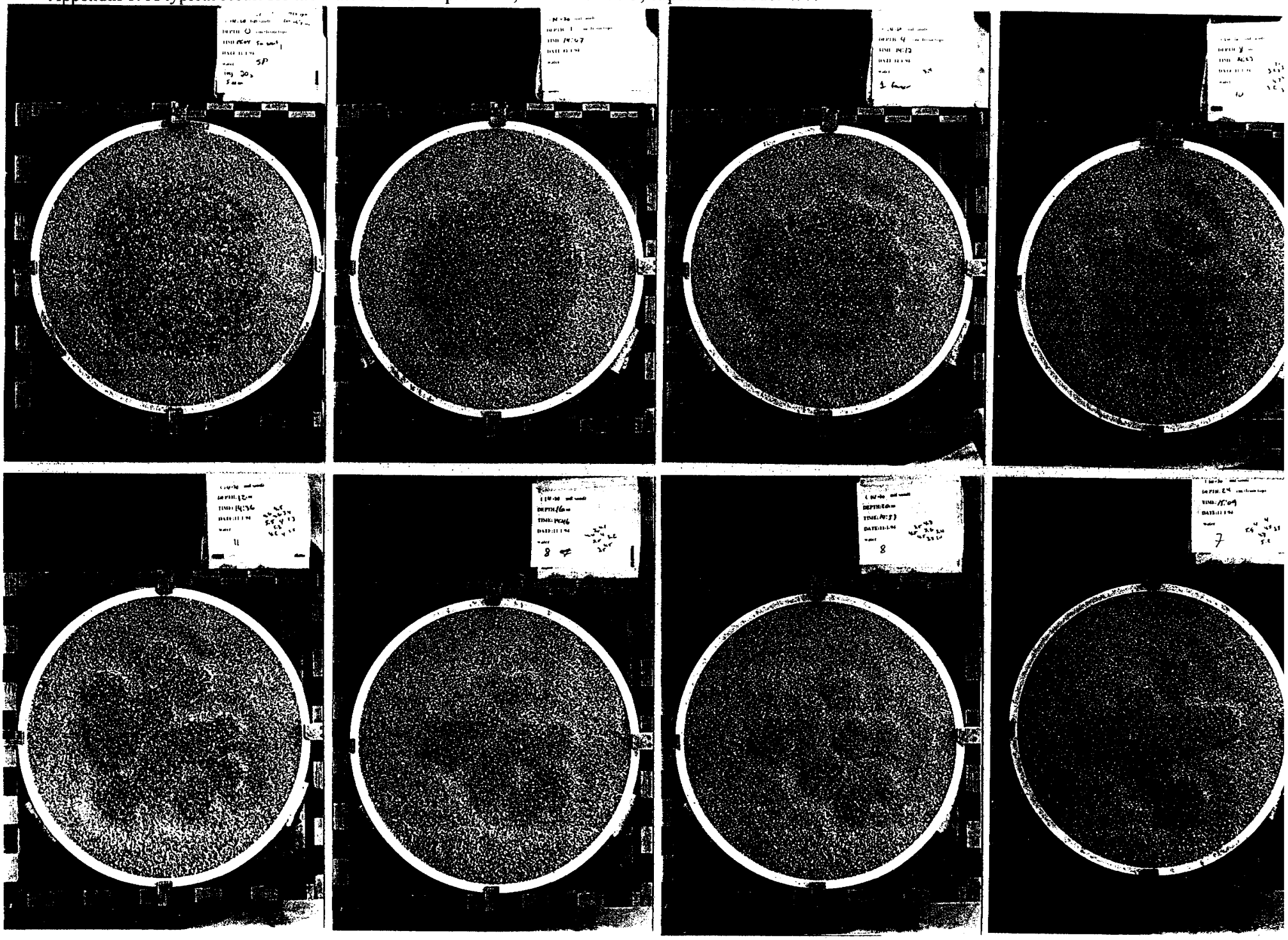

Appendix 6 continued